NAVAL POSTGRADUATE SCHOOL
MONTEREY, CALIFORNIA

THESIS

ASSESSMENT OF GRAIN REFINEMENT BY MICROTEXTURE ANALYSIS IN THERMOMECHANICALLY PROCESSED AL 2519 ALLOY

Steven L. Stancy

December, 1995

Thesis Advisor: T. R. McNelley

19960402 114

DTIC QUALITY INSPECTED 1

DISCLAIMER NOTICE

UNCLASSIFIED

Technical Report
distributed by

**DEFENSE
TECHNICAL
INFORMATION
CENTER**

DTIC/ Acquiring Information-
Imparting Knowledge

Cameron Station
Alexandria, Virginia 22304-6145

UNCLASSIFIED

THIS DOCUMENT IS BEST
QUALITY AVAILABLE. THE
COPY FURNISHED TO DTIC
CONTAINED A SIGNIFICANT
NUMBER OF PAGES WHICH DO
NOT REPRODUCE LEGIBLY.

REPORT DOCUMENTATION PAGE

Form Approved OMB No. 0704-0188

1. AGENCY USE ONLY *(Leave blank)*	2. REPORT DATE December 1995	3. REPORT TYPE AND DATES COVERED Master's Thesis

4. TITLE AND SUBTITLE Assessment of Grain Refinement by Microtexture Analysis in Thermomechanically Processed Al 2519 Alloy	5. FUNDING NUMBERS
6. AUTHOR(S) Steven L. Stancy	

7. PERFORMING ORGANIZATION NAME(S) AND ADDRESS(ES) Naval Postgraduate School Monterey, CA 93943-5000	8. PERFORMING ORGANIZATION REPORT NUMBER

9. SPONSORING/MONITORING AGENCY NAME(S) AND ADDRESS(ES)	10. SPONSORING/MONITORING AGENCY REPORT NUMBER

11. SUPPLEMENTARY NOTES The views expressed in this thesis are those of the author and do not reflect the official policy or position of the Department of Defense or the U.S. Government.

12a. DISTRIBUTION/AVAILABILITY STATEMENT Approved for public release; distribution is unlimited.	12b. DISTRIBUTION CODE

13. ABSTRACT *(maximum 200 words)*

The first part of this study involved determining the mechanism by which elevated-temperature deformation occurred for selected tensile specimens from previous research on thermomechanically processed Al 2519 alloy. Microtexture information in the form of discrete pole figures indicated that the most highly superplastic material had completely recrystallized and deformed via grain boundary sliding, whereas material that did not display superplastic behavior deformed via slip. The second part of the study was designed to achieve further refinement of the microstructure of Al 2519 using the particle stimulated nucleation (PSN) model as a guide. Using the overaging parameters of the thermomechanical process (TMP) that had yielded the greatest elongation in previous work, additional material was processed but with varying final total processing strain. The resulting material was analyzed using backscatter electron (BSE) microscopy methods to evaluate the effect of total processing strain on the average grain size. The smallest true volume grain size was associated with the material with the highest total processing strain.

14. SUBJECT TERMS BKD Patterns, Discrete Pole Figures, Grain Refinement	15. NUMBER OF PAGES * 66
	16. PRICE CODE

17. SECURITY CLASSIFICATION OF REPORT Unclassified	18. SECURITY CLASSIFICATION OF THIS PAGE Unclassified	19. SECURITY CLASSIFICATION OF ABSTRACT Unclassified	20. LIMITATION OF ABSTRACT UL

NSN 7540-01-280-5500

Standard Form 298 (Rev. 2-89)
Prescribed by ANSI Std. 239-18 298-102

ASSESSMENT OF GRAIN REFINEMENT
BY MICROTEXTURE ANALYSIS
IN THERMOMECHANICALLY PROCESSED
AL 2519 ALLOY

Steven L. Stancy

Lieutenant, United States Navy

B.S., Northwestern University, 1987

Submitted in partial fulfillment

of the requirements for the degree of

MASTER OF SCIENCE IN MECHANICAL ENGINEERING

from the

NAVAL POSTGRADUATE SCHOOL

December 1995

Author: _____
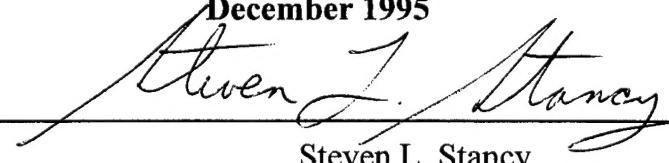
Steven L. Stancy

Approved by: _____
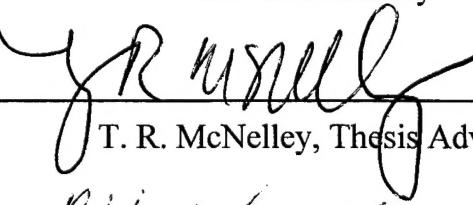
T. R. McNelley, Thesis Advisor

_____

Matthew D. Kelleher, Chairman

Department of Mechanical Engineering

iii

ABSTRACT

The first part of this study involved determining the mechanism by which elevated-temperature deformation had occurred for selected tensile specimens from previous research on thermomechanically processed Al 2519 alloy. Microtexture information in the form of discrete pole figures indicated that the most highly superplastic material had completely recrystallized and deformed via grain boundary sliding, whereas material that did not display superplastic behavior deformed via slip. The second part of the study was designed to achieve further refinement of the microstructure of Al 2519 utilizing the particle stimulated nucleation (PSN) model as a guide. Using the overaging parameters of the thermomechanical process (TMP) that had yielded the greatest elongation in previous work, additional material was processed but with varying final total processing strain. The resulting material was analyzed using backscatter electron (BSE) microscopy methods to evaluate the effect of the total processing strain on the average grain size. The smallest true volume grain size was associated with the material with the highest total processing strain.

TABLE OF CONTENTS

LIST OF FIGURES

LIST OF TABLES

I. INTRODUCTION

Superplasticity is a phenomenon whereby a metal exhibits extreme tensile ductility and deformation at relatively low stresses. An elongation of more than 200% is considered superplastic. First reported in 1934, an elongation of 1950% was obtained with a Si-Bi alloy [Ref. 1]. It was not until the 1960's, however, that research began in earnest in this field. Ductilities in excess of 5000% [Ref. 2] have been attained as the requirements for superplastic behavior and the associated processing and testing conditions have become better understood.

High tensile ductility suggests ease in forming and thus is the basis for practical application of this phenomenon. Superplasticity allows for complex shapes to be formed from a single sheet of superplastically processed material under specific fabricating conditions. Forming methods are similar to gas-pressure molding of plastic sheet material. Made as a single part, a component will have reduced need for fasteners, which can ultimately reduce fatigue and corrosion susceptibility. In addition, reductions in assembly time will lead to lower manufacturing costs. Current processing methods are alloy specific and result in materials that require elevated temperatures and low forming rates. The most highly superplastic Al alloys require expensive alloy modifications and exhibit only moderate mechanical properties. Current research seeks to devise superplastic processes that are economical and more widely applicable to existing commercially available Al alloys.

Military applications of superplastic materials are predominately in the aerospace sector. Current applications include space shuttle external fuel tank components, landing gear doors for the B-1 bomber [Ref. 3], various F/A-18A Hornet aircraft components [Ref. 4], and lightweight coolant piping and fire control radar dishes [Ref. 5] to name a few.

The first part of this research is an investigation into the mechanisms for selected samples of previously processed Al 2519 material that have demonstrated moderate superplastic behavior. Discrete pole figures were generated using backscatter Kikuchi diffraction patterns for microtexture analysis. The second part of this thesis attempts to create a microstructure that is likely to improve the superplastic response attained with Al 2519 alloy using Humphreys' particle stimulated nucleation (PSN) model as a guide to design a suitable process for this material.

II. BACKGROUND

A. ALUMINUM ALLOYS

Aluminum was of interest in this research because of its numerous desirable properties which include low density, high potential weight to strength ratio, high thermal and electrical conductivities, corrosion resistance, and relatively high ductility. Military applications such as aircraft and light armor often require components that are strong and yet lightweight. Because these components are often fabricated from several individual parts, the manufacturing time, and hence cost, are relatively higher than if they were fabricated in the form of a single piece. Assemblies of separate parts also require fasteners, either bolts or rivets, which function as stress raisers and lead to fatigue. Manufacturing of such strong, lightweight components in single units, though, can only be done with a material that possesses exceptional ductility. These reasons dictated the interest in making Al 2519 behave superplastically.

The Al 2519 alloy was originally developed specifically to be a weldable, moderately strong material. The alloy was selected specifically because of its availability and good overall strength characteristics. It is currently the strongest weldable aluminum alloy available. This alloy is wrought and contains 6.06 wt. pct. Cu which facilitates weldability because the backfilling eutectic liquid can seal cracks that may develop during weld metal solidification. The equilibrium phase diagram for the Al-Cu system is shown in Figure 2.1 [Ref. 6]. The Cu content actually exceeds the maximum solubility limit of Cu in the terminal Al solid solution, and, hence, there will be some insoluble Θ-
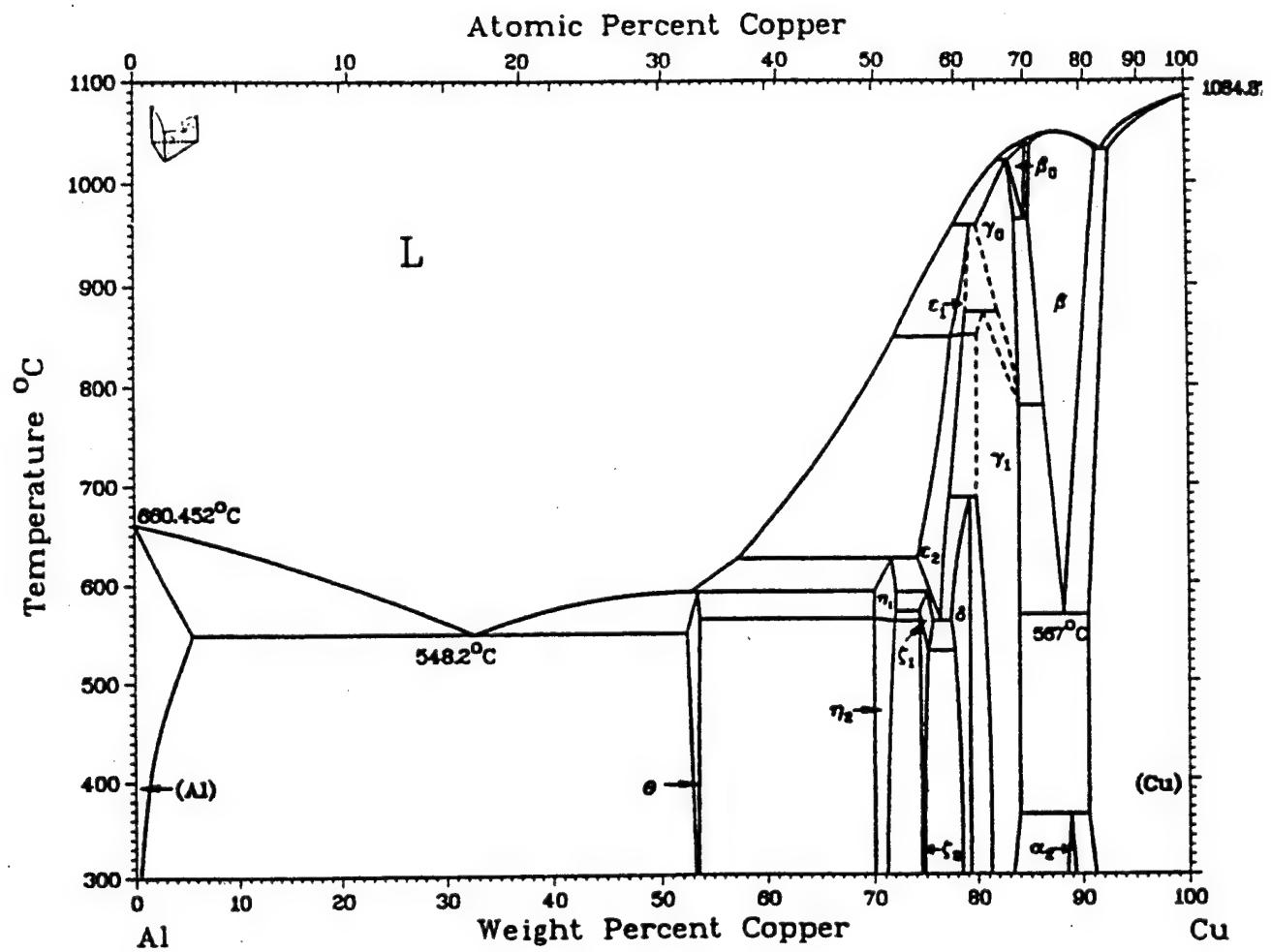
Figure 2.1: Al-Cu Phase Diagram [Ref. 6]

4

phase (Al$_2$Cu) at all processing or deformation temperatures up to the eutectic temperature ($\approx$548°C).

Because dislocations are relatively mobile in a pure metal, plastic deformation usually occurs readily via dislocation motion. To increase to strength of a pure metal, it is necessary to restrict dislocation movement by creating as many barriers as possible. This is usually done by one of three procedures: strain hardening, solid solution strengthening, and precipitation hardening. Strain hardening results from plastic deformation where dislocations are created that interact with one another which restricts their subsequent movement. Solid solution strengthening results from local strain fields that develop around substitutional solute atoms within a host matrix. The greater the size difference between the host and substitutional atom, the larger the resulting strain field (the Cu atom is approximately 11% smaller than the Al atom) [Ref. 7]. Strength results from the strain field interacting with edge dislocation stress fields, thereby inhibiting dislocation motion. When the solubility limit of a solute in a host matrix is reached, precipitate particles form, which lead to precipitation hardening.

Because Al 2519 contains 6.06 wt. pct. Cu, compared to the solubility limit of 5.65 wt. pct., the main strengthening mechanism for this alloy is precipitation hardening. As the material is cooled from the solution heat treatment temperature, the Cu atoms precipitate out from the host α-phase [Ref. 8]. Rapidly quenching the material from the elevated temperature, however, creates a supersaturated solid solution of Cu atoms in the Al matrix. Aging at a moderate temperature may result in the development of a series of metastable phases before the formation of the stable Θ-phase as shown:

5

$$SSS \rightarrow \alpha + GP\ I \rightarrow \alpha + GP\ II \rightarrow \alpha + \Theta`` \rightarrow \alpha + \Theta` \rightarrow \alpha + \Theta\ (Al_2Cu)\ .$$
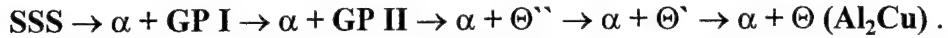
Peak strength is usually associated with the formation of $\Theta``$ or $\Theta`$. Precipitate particles

of the stable Θ-phase will be shown to possibly function as nucleation sites for

recrystallization if they are of a sufficient size [Ref. 9].

B. COMMERCIAL PROCESSING METHODS

Materials are not naturally superplastic. Instead, they must be processed to

exhibit this behavior. There are currently two superplastic processing methods for Al

alloys. Each of these methods, though, is only applicable for one specific alloy. The first

procedure, developed by British Aluminum (now British Alcan Aluminum plc.) is a

thermomechanical process (TMP) for the Al-Cu-Zr (Supral) alloy. The second process,

developed at the Rockwell International Science Center, is a TMP designed for the Al-

Zn-Mg-Cu (Al 7475) alloy.

1. Supral Process

The Supral process begins with an Al-Cu alloy and adds a third alloying element,

Zr, which enables a uniform dispersion of very fine $ZrAl_3$ particles to precipitate. This

second phase dispersion inhibits grain boundary migration, and thereby limits grain

growth at elevated temperatures.

There are four basic steps to the Supral process. The first step is to melt the

material at a high temperature. Because of the peritectic at the Al end of the Al-Zr

binary-phase diagram, an extremely high melting temperature must be used to prevent the

formation of primary $ZrAl_3$. The material is chill cast and then hot worked under strictly

controlled temperature and time conditions to ensure that the $ZrAl_3$ particles remain finely dispersed throughout the Al matrix. At $300^{o}C$, warm rolling to a 90% reduction follows. Recovery and recrystallization are inhibited by the $ZrAl_3$ particles, and Cu and Mg phases to a lesser degree, that precipitate from solution. Cold working next creates a high strain energy in the material prior to the final step of continuous recrystallization during deformation at approximately $450^{o}C$. [Ref. 10]

2. Rockwell Process

The TMP designed by the Rockwell International Science Center is also a four-step process beginning with a solution heat treatment at $482^{o}C$ for three hours to dissolve the Zr and Mg solutes and create a homogeneous single-phase solid solution. The material is then quenched to room temperature which results in a supersaturated solid solution. The second step is an overaging process at $400^{o}C$ for eight hours which produces an equilibrium M-phase with particles of about 0.75 μm size intended to act as nucleation sites for recrystallization. After a quench to room temperature, the material is deformed and then recrystallizes at $482^{o}C$, which produces a grain size of approximately 10 μm in diameter. It is imperative that the final heating rate be sufficiently fast to prevent grain growth that appears to occur if the rate is too slow. [Ref. 11]

C. FEATURES OF SUPERPLASTICITY

Analysis has revealed that there are certain common characteristics shared by most materials that exhibit superplastic behavior. First, most superplastic materials possess a fine, equiaxed grain size that is less than or equal to 10 μm in size. A fine grain

size permits easier grain boundary sliding with associated grain rotation [Ref. 12], the importance of which will be seen later. This fine grain size may be stable when the volume fraction of second-phase precipitate particles is relatively high. Superplastic behavior also occurs only when the deformation temperature exceeds approximately one half the material's melting temperature, and the deformation strain-rate is between $\sim 10^{-2}$ and 10^{-4} sec^{-1}. Another common quality is a relatively high strain rate sensitivity coefficient, m, between 0.3 and 0.9; the higher values correspond to a finer grain size. Superplastic materials also do not exhibit localized necking but rather a uniform reduction in thickness during deformation as a result of deformability by grain boundary sliding with accompanying grain rotation. Grain boundary sliding is accompanied by a reduction in preferred orientation, or texture. Any texture remaining after large superplastic deformations is likely the result of slip occurring within individual grains as a consequence of the applied tensile stress. Failure occurs, however, as a result of cavitation around the coarser precipitate particles. Transmission electron microscopy has revealed a lack of dislocations in superplasticly deformed material possibly because dislocations need to travel only a short distance (≤ 1 μm) to reach grain boundary sinks. [Ref. 1]

D. PARTICLE STIMULATED NUCLEATION (PSN) THEORY

One of the common characteristics of superplastic materials is a grain size on the order of or less than 10 μm [Ref. 1]. To produce a refined grain size, a material must have a high density of nucleation sites, and the presence of well-dispersed precipitates of

a critical size in a matrix has been seen to promote recrystallization. From observations involving materials containing non-deformable second-phase particles, Humphreys concluded that the precipitate particles must be of a critical size for a given reduction in order that the particles act as nucleation sites. During deformation, the host matrix will flow around non-deforming, equiaxed particle if void formation is not to occur. This creates a deformation zone containing a quantity of dislocations. The overall density of these dislocations can be estimated from equation (1) [Ref. 13]:

$$\rho_g = \frac{8 f \cdot \gamma}{b \cdot d_p} \tag{1}$$

where f represents the volume fraction of the precipitate phase, γ the shear strain, b the Burgers vector, and d_p the particle diameter. These dislocations provide strain energy in the deformation zone that is minimized by alignment of like-sign dislocations to create subgrains with local lattice rotations. The subgrain, or recrystallization embryo, that contains the highest dislocation density may form a recrystallized grain before neighboring embryos because it has the largest driving force. Humphreys observed that small particles ($d_p < 0.1$ μm) and low strains resulted in prismatic loops near the precipitate which did not provide the necessary lattice reorientation for PSN. However, large particles ($d_p > 0.1$ μm) and larger strains resulted in the dislocation structures necessary to produce sufficient local lattice reorientation. Theoretically, in order for the embryo to form a new grain and grow into the surrounding matrix it must be of sufficient size, δ_{crit}, defined by equation (2) [Ref. 14]:

$$\delta_{crit} = \frac{4 \cdot \Gamma}{E} \tag{2}$$

where Γ is the grain boundary interfacial energy and E is the stored strain energy from deformation.

In addition, the critical size of the embryo, δ_{crit}, must also be smaller than the deformation zone, λ, that is created near the precipitate particle such that $\delta_{crit} < \lambda$ [Ref. 9]. During straining, the size of the deformation zone is approximated by equation (3) [Ref. 13]:

$$\lambda = A \cdot d_p \cdot \varepsilon^{\frac{n}{n+1}} \tag{3}$$

where λ is the width of the deformation zone, A is a material constant, ε the true axial strain, and n is the exponent from Holloman's strain hardening equation, equation (4):

$$\sigma = K\,\varepsilon^n \tag{4}$$

where σ is the true stress. As the deformation zone size, λ, increases in size, more embryos achieve conditions for nucleation. Increasing d_p and/or ε will increase λ, and, therefore, allow more embryos to satisfy this requirement.

From equations (2) and (3), a relationship between particle size and strain necessary for PSN becomes:

$$A \cdot d_{p,crit} \cdot \varepsilon^{\frac{n}{n+1}} = \frac{4 \cdot \Gamma}{E} \tag{5}$$

or

$$d_{p,crit} = \frac{4 \cdot \Gamma}{A \cdot E} \cdot \frac{1}{\varepsilon^{\frac{n}{n+1}}} \ . \tag{6}$$

Thus, as the true strain increases, the critical particle diameter necessary for PSN decreases as shown in Figure 2.2 [Ref. 9].
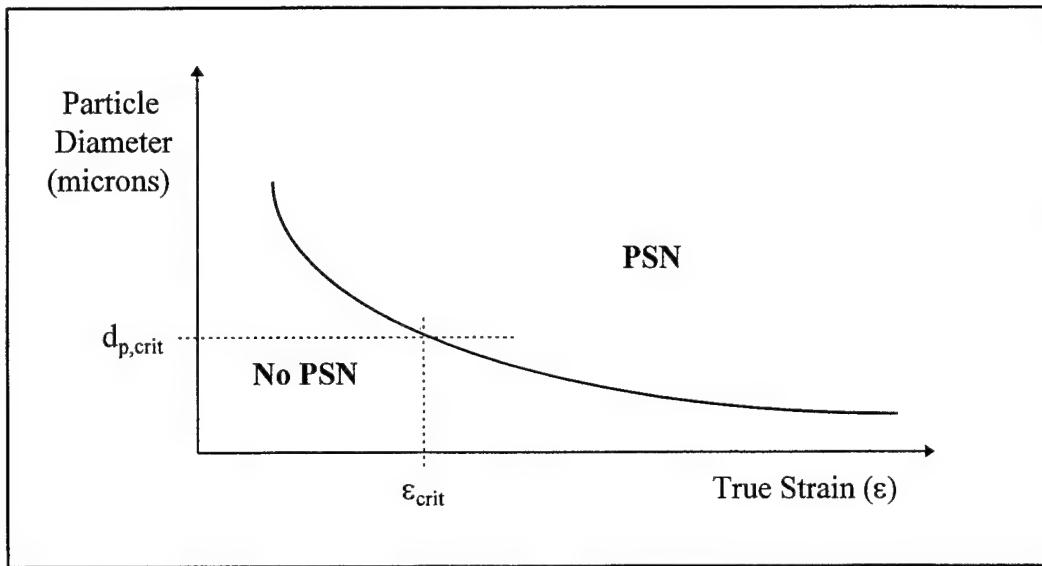
Figure 2.2: Particle Size and True Strain Relationship Necessary for PSN

Assuming that all nucleated grains grow until impingement with a neighboring grain, and that all particles are of the same size, where $d_p \geq d_{p,crit}$, the resultant grain size associated with a given precipitate particle size can be approximated by equating the grain size to the particle spacing, D_s [Ref. 15]:

$$D_s = \frac{d_p}{f^{1/3}} \ .$$ (7)

Equation (7) shows that for the grain size, D_s, to be a minimum, the particle size must be a minimum (but $\geq d_{p,crit}$) for a given volume fraction, f.

Nucleation must also occur at an appreciable rate, r, for recrystallization to take place. The rate of nucleation follows the relationship in equation (8):

$$r = A \cdot e^{-\frac{\Delta G^*}{kT}}$$ (8)

11

where ΔG^* is the free energy of formation of a nucleus. For a high nucleation rate, the second term must be small which means that ΔG^* must be small and kT large. It is necessary, therefore, that the processing temperature be as high as possible.

E. RESEARCH AT NPS

Recent research on thermomechanical processing at the Naval Postgraduate School (NPS) has sought, among others things, to devise processes that produce a superplastic response in existing Al-based alloys in order to avoid the addition of special alloying elements and the associated additional complexities and manufacturing costs. The PSN model previously described has been used in an effort to produce a microstructure that has both a fine grain size and large misorientation angle between neighboring grains, the two microstructural components believed necessary for superplastic behavior. Initially, an Al-10Mg-0.1Zr alloy was studied and has produced elongations of approximately 1100% at a tensile test temperature of 300°C. This alloy, however, represents a model system and subsequent efforts have examined Al 2519, an Al-6.0Cu material.

Mathe initiated the research by employing a modified version of the TMP used with the Al-10Mg-0.1Zr alloy [Ref. 16]. Different combinations of cold rolling and overaging conditions were utilized to develop a superplastic microstructure similar to that found with the processed Al-10Mg-0.1Zr alloy. The greatest ductility, 205% elongation, was obtained when a 10% prestrain at 200°C was applied to the material prior to overaging at 450°C for 10 hours. This TMP also produced a uniformly distributed Θ-

phase of 1-2 μm size which was the size determined necessary for PSN [Ref. 9]. Bohman continued Mathe's work by adjusting overaging conditions [Ref. 17]. By increasing the overaging time at 450°C to 50 hours, a significantly larger number of particles achieved a size greater than 1 μm which resulted in a refined grain size and an increased ductility of 260%. Dunlap further increased the overaging time from 50 hours to 100 hours and reduced the rolling temperature from 300 to 200°C to increase the stored strain energy [Ref. 18]. Neither of these changes resulted in further grain refinement. Zohorsky studied the effect of prestrain deformation temperature, overaging temperature, and other TMP variations on the production of Θ-phase particles exceeding a critical size [Ref. 19]. It was concluded that a 10% prestrain performed at room temperature instead of at 200°C produced a more uniform distribution of Θ particles, and that the conditions of 50 hours at 200°C and 50 hours at 400°C produced the most promising microstructure. Peet subsequently varied the overaging temperature and times prior to rolling in an effort to further refine the grain size and varied the tensile test temperatures to further examine superplastic response [Ref. 20].

The preceding research sought to create a microstructure that contained precipitate particles of a critical size that would function as nucleation sites for recrystallization when subjected to a processing strain. In all cases, materials were rolled to strains of approximately 2.2 as dictated by initial billet thickness and available facilities. Moderate superplastic ductilities up to 300% resulted from these studies. To refine the grain size further, more of the precipitate particles must become active as nucleation sites. According to the PSN model, this can also be achieved by increasing the total processing

strain on the material. In fact, McNelley et al. concluded that by increasing the processing strain on Al-10Mg-0.1Zr from 1.9 to 2.6 an increase in peak ductility from 450 to 1100% resulted [Ref. 15], which is in agreement with the PSN model. The current research with Al-6.0Cu seeks to determine the effect that processing strain has on grain refinement and superplastic ductility.

F. BACKSCATTER KIKUCHI DIFFRACTION (BKD) PATTERNS

In an effort to understand the mechanism by which deformation had occurred in previous studies, electron backscatter patterns (EBSP) were generated in a scanning electron microscope (SEM) from selected samples of processed Al 2519 tension test specimens. These EBSPs, when generated in the SEM, are known as backscatter Kikuchi diffraction (BKD) patterns. The equipment hardware configuration used to generate, collect, and process the BKD patterns is presented in Figure 2.3.

When the electron beam is incident upon the sample, some electrons will be inelastically scattered and diffracted back (backscattered) through the specimen surface and toward the electron source according to Bragg's law [Ref. 21]. The sample is positioned so that its normal is at a relative angle of 70° to the incident beam. This increases the intensity of the diffracted electrons and facilitates detection of the Kikuchi bands that are generated. A phosphor screen placed approximately 40 mm from the specimen provides a means to detect and display the resultant Kikuchi bands. The intersection of Kikuchi bands defines the location of crystallographic zone axes. These bands will form a pattern, part of a Kikuchi map, that is fixed to a specific crystal lattice,
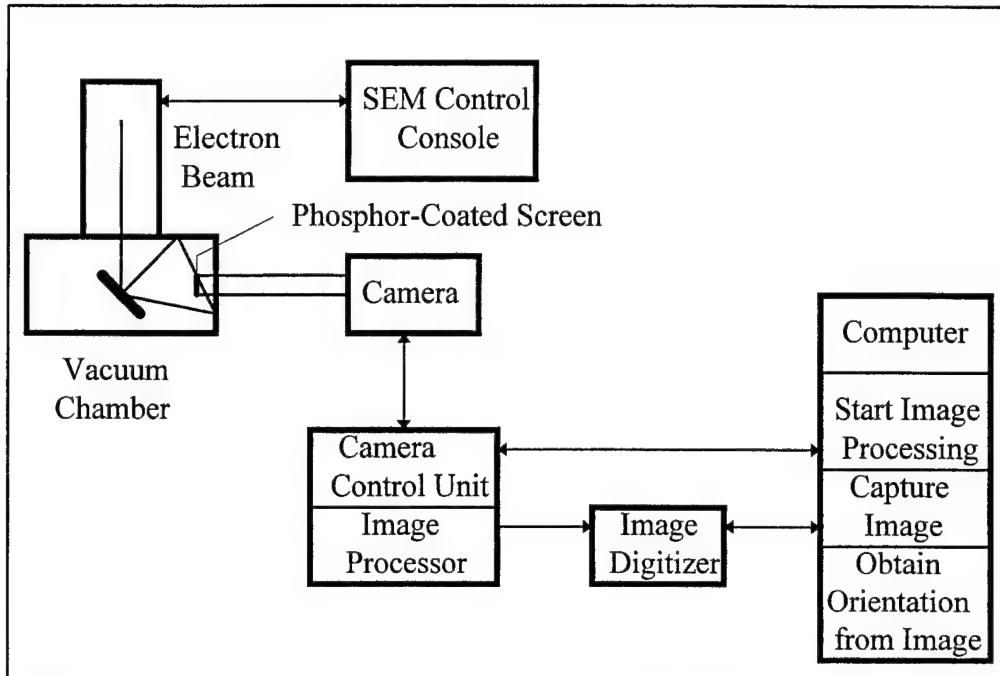
Figure 2.3: Equipment Configuration for Generating BKD Patterns

and as the crystal is rotated, so is the pattern. Therefore, as the electron beam is displaced

from one grain to another, the pattern will shift accordingly. The pattern can appear to

rotate or translate, or both, depending on the type of boundary between the grains. The

specific pattern for a given grain provides orientation information about the crystal

lattice. The pattern that is projected onto the phosphor screen is viewed by a fiber optic

camera which sends the image through a camera control unit (CCU), where the image

quality is enhanced, to a monitor for display as seen in Figure 2.4 (a). Next, a computer

workstation "captures" the image so that the crystal lattice orientation can be determined,

or indexed, and the results saved for further analysis. BKD patterns can be indexed one

of four different ways, two automatically and two manually for improved accuracy when

the image quality is poor. The indexing routines use either the Hough transform

algorithm, which measures the angles between Kikuchi bands, i.e., the angle between

15

crystal planes, or the Burns algorithm, which measures the position and width of pairs of

Kikuchi bands. The software will superimpose a series of lines over the observed

Kikuchi bands to indicate the computed crystal orientation as displayed in Figure 2.4 (b).

The crystal orientation is saved by the software in terms of three Euler angles, φ_1, ϕ, and

φ_2, representing consecutive rotations that will bring a global reference system

corresponding to the specimen's normal direction, rolling direction, and transverse

direction, respectively, into coincidence with the cube axes of the local crystal lattice.

These angle measurements are accurate to within $0.5°$ [Ref. 22]. The crystal lattice

orientations can be used to extract a wide range of information about the material

including an understanding of the mechanism by which deformation occurred when

subjected to an axial stress.
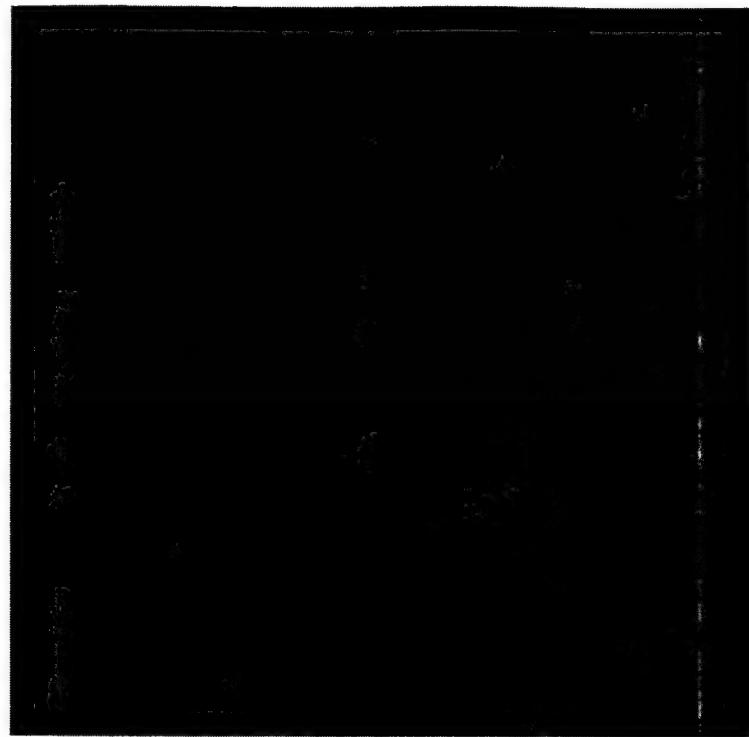
(a)
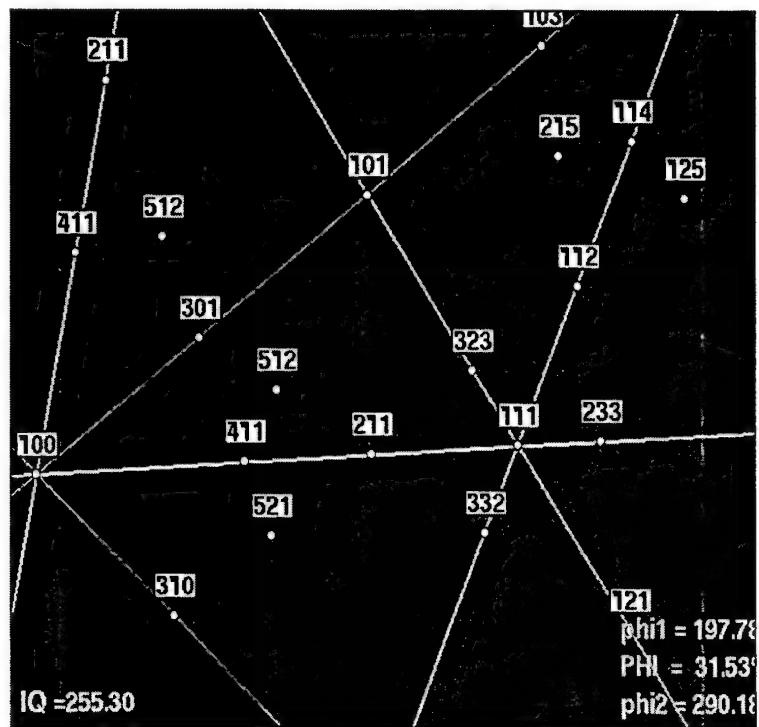
(b)

Figure 2.4: BKD Pattern from Silicon Crystal.
(a) Unindexed; (b) Indexed.

17

III. EXPERIMENTAL PROCEDURE

A. MATERIAL

The material used in this research was obtained from the Aluminum Company of America (ALCOA) Technical Center, ALCOA Center, Pennsylvania and is the same material as used in previous work on Al 2519. The alloy was received in the form of a rolled plate of 1.5 inches in thickness and tempered to the T87 condition; this temper indicates that the material had been solution heat treated at 535°C, cold rolled to a seven percent reduction, and then artificially aged for 24 hours at 165°C [Ref. 8]. The composition of the 2519 alloy is listed in Table 3.1.

Cu	Mn	Mg	Fe	Zr	V	Si	Ti	Zn	Ni	Be	B	Al
6.06	0.30	0.21	0.16	0.13	0.09	0.07	0.06	0.03	0.01	0.002	0.001	bal

Table 3.1: Aluminum Alloy 2519 Composition (Weight Percent)

B. PROCESSING

Prior to processing the as-received material, the plate was sectioned into billets with average dimensions of 63.5x38.1x30.0 mm (2.50x1.50x1.18 inches) where the largest dimension was in the prior rolling direction. The 1.18 inch thickness was achieved by milling an equal amount of material from the top and bottom of the as-

19

received plate. Each sample was stamped after initial milling with a number to distinguish it from the others.

The thermomechanical processing of the material consisted of the eight steps that are outlined in Figure 3.1. All samples were initially solution heat treated at 535°C for 130 minutes in a Lindberg Blue M box furnace (Model 51442) to return the Cu alloying addition into solution [Ref. 23]. Thermocouples were placed in close proximity to each

```
┌─────────────────────────────────────────────────────┐
│              ┌──────────────────────┐                │
│              │     Solutionize      │                │
│              │     130 minutes      │                │
│              │      at 535°C        │                │
│              └──────────┬───────────┘                │
│                         ▼                            │
│         ┌───────────────────────────────┐            │
│         │ Water quench to room temperature │          │
│         └───────────────┬───────────────┘            │
│                         ▼                            │
│           ┌─────────────────────────┐                │
│           │ Prestrain 10% at room temp │              │
│           └───────────┬─────────────┘                │
│                       ▼                              │
│          ┌──────────────────────────┐                │
│          │ Overage at 200°C for 50 hours │           │
│          └────────────┬─────────────┘                │
│                       ▼                              │
│         ┌───────────────────────────┐                │
│         │ Overage at 450°C for 100 hours │           │
│         └─────────────┬─────────────┘                │
│                       ▼                              │
│            ┌─────────────────────┐                   │
│            │ Furnace cool to 200°C │                 │
│            └──────────┬──────────┘                   │
│                       ▼                              │
│         ┌───────────────────────────────┐            │
│         │ Water quench to room temperature │          │
│         └───────────────┬───────────────┘            │
│                         ▼                            │
│           ┌─────────────────────────┐                │
│           │ Heat to 200°C and warm roll │             │
│           │   to desired total strain.  │             │
│           │      See Table 3.2.         │             │
│           └─────────────────────────┘                │
└─────────────────────────────────────────────────────┘
```
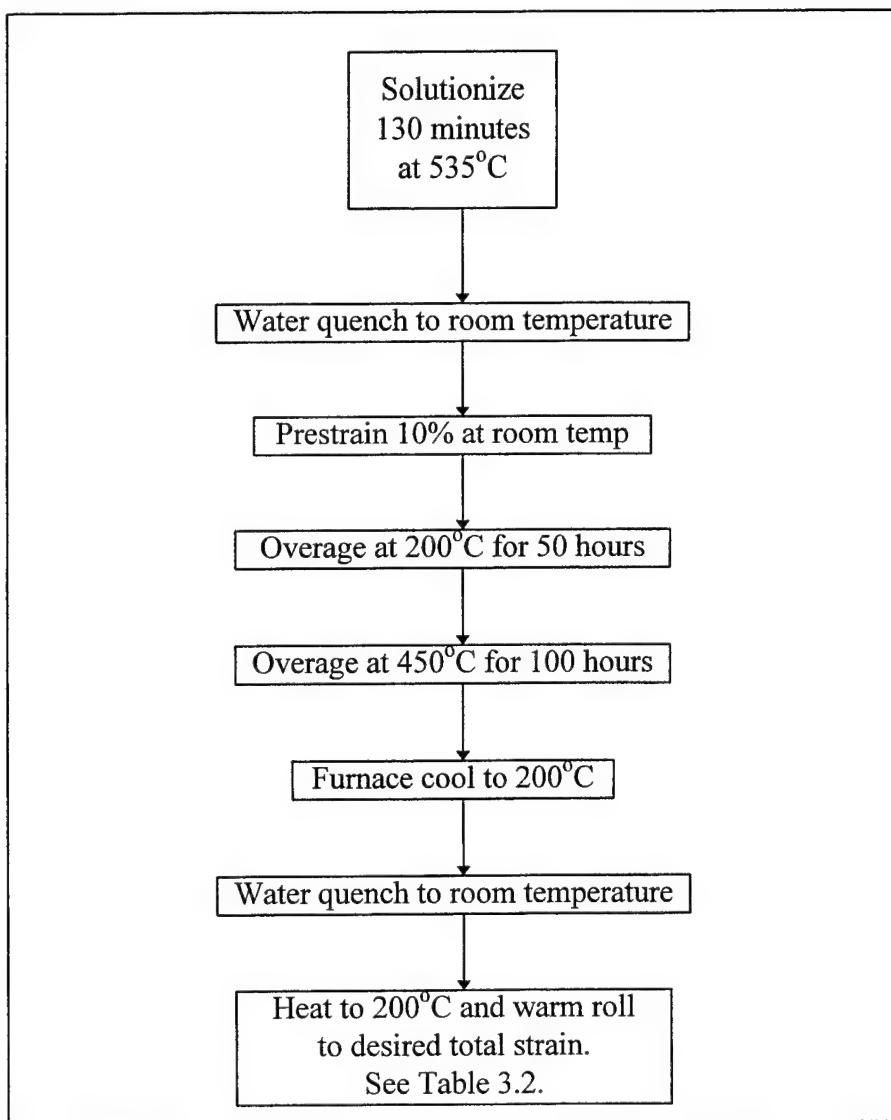
Figure 3.1: Thermomechanical Processing Steps

sample to ensure the necessary temperature was maintained during heat treatments. Following a water quench to room temperature, the material was cold rolled in three passes to a 9.6% cold reduction. This increased the dislocation density in the material in order to provide potential nucleation sites for Cu precipitation. Next, the material was artificially aged at 200°C for 50 hours and then at 450°C for 100 hours to allow the Cu to diffuse and provide a uniform dispersion of the resultant Θ particles. The prolonged aging was required to allow the Θ-phase particles to coarsen to a critical size necessary for PSN. The material was then furnace-cooled to 200°C, at a rate of approximately 1.0°C per minute, and then water quenched to room temperature. To this point, the TMP duplicated that which had lead to Peet's most highly superplastic material [Ref. 20]. Billets were stored in a freezer prior to subsequent rolling. A series of eighteen warm rolling passes on a Fenn laboratory mill (4.0 inch roll diameter) followed. Each pass was followed by a 30-minute anneal at 200°C as detailed in Table 3.2. The mill gap setting on the mill was done using prefabricated gage blocks in combination with standard feeler gages. All thicknesses were confirmed with a standard micrometer.

The true strain for each warm rolling pass is included in Figure 3.2. Thickness reductions for the first twelve passes were small to prevent the material from alligatoring (splitting in half in the transverse/rolling direction plane). After warm rolling pass number four (W4), the material was water quenched to room temperature, and 6.35 mm (0.25 inch) was removed from the billet ends with a band saw. This removed stress raisers that developed as the ends formed an "hour- glass" shape from the rolling process. After warm rolling pass number eight (W8), the material was again water quenched to

21

Roll Pass #	Initial Thickness (in)	Mill Gap Setting (in)	Final Thickness (in)	Mill Deflection (in)	True Strain ε	Total Strain ε_{total}
C1	1.180	1.095	1.123	0.028	0.050	/
C2	1.123	1.049	1.077	0.028	0.042	/
C3	1.077	1.045	1.073	0.028	0.004	/
W1	1.073	0.985	1.006	0.021	0.064	0.064
W2	1.006	0.925	0.948	0.023	0.059	0.124
W3	0.948	0.865	0.890	0.025	0.063	0.187
W4	0.890	0.805	0.828	0.023	0.072	0.259
W5	0.828	0.745	0.770	0.025	0.073	0.332
W6	0.770	0.685	0.712	0.027	0.078	0.410
W7	0.712	0.625	0.652	0.027	0.088	0.498
W8	0.652	0.565	0.593	0.028	0.095	0.593
W9	0.593	0.505	0.530	0.025	0.112	0.705
W10	0.530	0.445	0.472	0.027	0.116	0.821
W11	0.472	0.389	0.417	0.028	0.124	0.945
W12	0.417	0.332	0.364	0.032	0.136	1.081
W13	0.364	0.234	0.266	0.032	0.314	1.395
W14	0.266	0.153	0.185	0.032	0.363	1.758
W15	0.185	0.088	0.125	0.037	0.392	2.150
W16	0.125	0.042	0.078	0.036	0.472	2.622
W17	0.078	0.012	0.047	0.035	0.507	3.128
W18	0.047	0.012	0.039	0.027	0.187	3.315

**Table 3.2:** Rolling Schedule
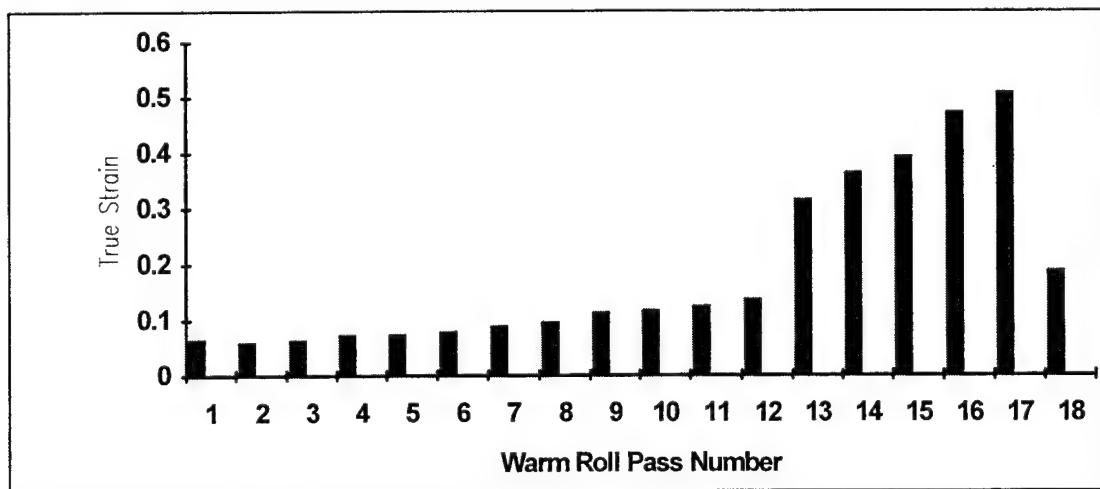
Figure 3.2: True Strain (ε) vs. Warm Rolling Pass

room temperature, after which 6.35 mm (0.25 inch) was removed from the ends and sides to eliminate newly developed stress raisers. The strain per pass increased in passes 13-17. Pass eighteen brought the material to the desired final thickness and total processing strain. To ensure straightness, the billets were rotated 180° about the longitudinal axis on each successive pass; also, billets were returned to the furnace in such a manner to result in alternating ends entering the roll gap on successive passes. The material was water quenched to room temperature after completing the warm rolling.

To analyze the effect of total processing strain on grain size, one sample was warm rolled only through W13, while a second was rolled through W15, and the third through W18. The total processing strain values attained were 1.4, 2.2, and 3.3, respectively.

Three specimens, approximately 1 cm square in size, were then sectioned from each finished rolling product using a Buehler Isomet high speed saw. At 2500 rpm, the 11-4217 abrasive wheel applied an 800 gram load on the specimen. ISOCUT PLUS Fluid cooled and lubricated the specimen and the cutting wheel and flushed away all cutting debris.

The final phase of processing involved annealing one sample from each of the three rolled materials at 400°C for either 0.5, 1.0, or 2.0 hours. The annealing temperature was selected because the finest grain size had been obtained by Peet at this temperature in his research [Ref. 20]. The annealing times roughly correspond to the time necessary for tensile testing at strain rates of 10^{-2}, 10^{-3}, and 10^{-4}, respectively.

C. METALLOGRAPHIC SAMPLE PREPARATION

The sectioned specimens were then ground using a Struers Knuth-Rotor-3 grinding wheel with Struers water-proof silicon carbide paper of grit increasing from 1000 to 2400 to 4000. Moderate pressure was applied to each specimen for 20-30 seconds per each grit stage. Polishing followed on 12 inch Buehler wheels rotating at 400 rpm. The specimens were polished first with 6.0 μm diamond compound on a Buehler MICROCLOTH polishing cloth for 30 seconds and then with 1.0 μm diamond compound on Buehler CHEMOMET cloth for 30 seconds. All polishing was done using Metadi Fluid as a lubricant. After each polishing stage, the specimen was rinsed with methanol and dried with cold air from a Buehler Torramet specimen dryer.

All specimens were then electropolished. The electrolyte solution, a 70% methanol/30% nitric acid mixture, was cooled to -20°C in a stainless steel beaker by placing it in an insulated methanol bath that was cooled with liquid nitrogen. The electrolyte was continuously stirred magnetically. Prior to placing the specimens in the electrolyte, a non-conducting lacquer was applied to the specimen surface area except for the area to be electropolished. Polishing was done by attaching the negative lead from the power supply to the beaker and attaching the positive lead to the specimen. With the power supply set at 7 volts, the specimen was placed in the solution for 1.5 minutes. After electropolishing, the specimen was rinsed with methanol and then air dried with cool air from the specimen dryer.

D. MICROSCOPY

The polished samples were placed in a TOPCON SM-510 scanning electron microscope operating in the backscatter mode. A 5.0 kV accelerating voltage and 1000X magnification were used in conjunction with a 10 mm working distance. The sample was placed perpendicular to the incident electron beam. Link ISIS and Tetra software on an attached personnel computer controlled the image contrast and brightness. Photomicrographs of the processed and annealed material showed good grain orientation contrast and Θ-phase particles. This procedure allowed grain size information to be obtained.

E. BACKSCATTER KIKUCHI DIFFRACTION (BKD)

To obtain orientation information, tensile specimens were placed in the SEM with the sample normal at a 70° angle from the incident electron beam. BKD patterns were obtained on a phosphor screen that is placed approximately 40 mm from the specimen in the SEM chamber (see Figure 3.3). The SEM was set for 1000X magnification and 20.0 kV accelerating voltage. The working distance was dependent upon the area of study. The main goal in adjusting the working distance was to maintain the geometry of the sample relative to the center of the phosphor-coated screen and to improve the image quality of the diffraction pattern. As the incident electron beam was moved from the grip to the gage section of the specimen, the platform was raised. The specimen with the greatest elongation required the platform to be raised proportionately higher. A limit, however, was created by the position of the objective lens. For all microtexture

measurements, the area of study was either in the center of the rectangular grip section or at the tip of the deformed gage section, i.e., at the fracture point.

Once the specimen was positioned, the secondary electron image was focused to improve the image quality of the diffraction pattern. From the camera control unit, background noise was "captured" for later subtraction. The "spot" option was then selected on the SEM console corresponding to a specific area ≈ 0.1 μm in extent on the sample. A fiber optic attachment to a low-light camera (viewing the backside of the phosphor screen) provided input to a monitor which displayed the BKD pattern. The BKD pattern appeared blurred until the background noise was subtracted from the image. The pattern of Kikuchi bands and the major zone axes then became clear. For this face-centered cubic (FCC) Al alloy, each pattern usually contained two of the following three major zone axes: <100>, <110>, and <111>. The pattern was "captured" by a Silicon Graphics Indy desktop computer using TexSEM Laboratories' (TSL) Automatic Pattern Recognition software (APR 1.5). After careful calibration of the software using recognized major zone axis, the APR software automatically indexed the pattern and saved the grain orientation information in the form of three Euler angles, φ_1, ϕ, and φ_2, with the z-axis corresponding to the normal of the specimen surface and the x-axis along the rolling direction/tensile axis. These three angles represent three consecutive rotations that bring the sample's global reference axes into concurrence with the local crystal lattice orientation. After the pattern was indexed and saved, the electron beam was magnetically deflected in increments of approximately 0.5 μm until either the pattern significantly shifted or a new pattern appeared on the monitor. The process was then

repeated. Because the sample was inclined at such a steep angle, only a small horizontal

section of the secondary electron image was in focus at one time. To ensure optimum

BKD pattern image quality, the secondary image was focused several times as the

electron beam was manually rastered over the specimen. This interactive procedure was

repeated randomly throughout the area of interest until five-hundred grain orientations

had been determined.
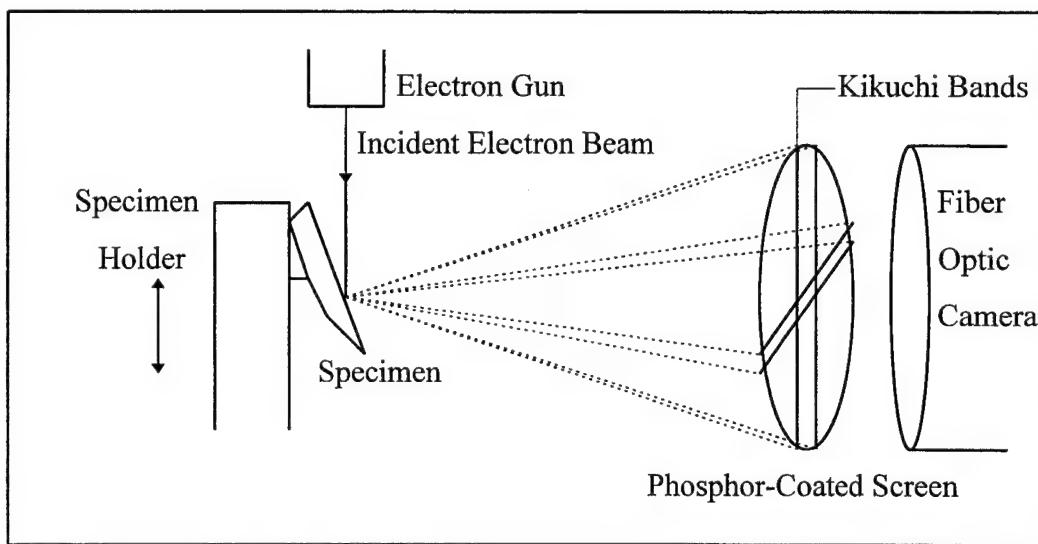
Figure 3.3: SEM Setup to Collect BKD Patterns

From the five-hundred grain orientations, a set of three discrete pole figures were

generated using the Hough transform algorithm in the TSL APR software. Prior to

plotting the pole figures, however, the projections had to be rotated twice. A 90° rotation

correction was necessary because the software default assumes the rolling plane normal

to be in the plane defined by the electron beam and the camera axis. The specimens used

in this research were viewed with the long-transverse direction in this plane. The second

rotation was a 40-50° correction to account for the helical path of the incident electron beam. The set of three discrete figures were finally plotted for each area of interest which revealed the orientation of the grain normals for the {111}, {200}, and {220} planes.

IV. RESULTS AND DISCUSSION

A. DISCRETE POLE FIGURE MEASUREMENTS

The initial phase of this research involved the use of backscatter Kikuchi diffraction (BKD) methods described in Chapter II to investigate deformation mechanisms in processed Al 2519 materials. A series of samples from previous work was selected for this purpose. In general, metals deform via intragranular slip whereby planes of atoms slide over adjacent planes of neighboring atoms; slip processes result in lattice rotations and preferred orientations [Ref. 1] [Ref. 24]. Superplastic materials, however, deform by another mechanism: grain boundary sliding [Ref. 1]. Here, the grains themselves slide past one another along their mutual boundaries. This process is facilitated by having a highly refined grain size on the order of or less than 10 μm [Ref. 1]. Deformation by grain boundary sliding tends to eliminate preferred orientations.

Five samples were chosen from previous research for analysis. Pertinent information on material processing history as well as elevated-temperature tensile testing response is listed in Table 4.1. The "/" mark indicates that those material processing and test conditions were not examined in this research. The true volume grain size, D, was evaluated using the mean linear intercept method (MLI) to obtain an initial grain size, d_{MLI}, and then multiplying by a correction factor of 1.776 ($D = d_{MLI} * 1.776$).

Overaging Conditions Prior to Warm Rolling of Thermomechanical Process		Tensile Testing Conditions						
		Strain Rate (sec^{-1})	300°C Test Temperature		400°C Test Temperature		450°C Test Temperature	
Temp (°C)	Time (hours)		elongation (%)	True Volume Grain Size, D (μm)	elongation (%)	True Volume Grain Size, D (μm)	elongation (%)	True Volume Grain Size, D (μm)
400	50	10^{-2}	/	/	187.6	21.0	/	/
400	100	10^{-3}	/	/	188.2	21.0	/	/
450	100	10^{-4}	143.3	19.5	196.3	11.2	296.4	17.0

Table 4.1: Elongation and True Volume Grain Size Data From Previous Work

1. Effect of Processing History

The effects of thermomechanical processing parameters, specifically the overaging temperature and time prior to the rolling, on elongation to failure as well as true volume grain size were of initial interest. For this analysis, the tensile test temperature of 400°C was held constant. The resultant ductilities of 187.6 and 188.2% were nearly identical for the prior overaging conditions of 400°C for either 50 or 100 hours. At 21.0 μm, the measured grain size was identical for both processing conditions. However, increasing the prior overaging temperature to 450°C for 100 hours resulted in considerable refinement of true volume grain size, to a value of 11.2 μm, but with only a slightly greater elongation of 196.3%.

These tensile specimen grip and gage sections were separately analyzed by the methods described in Chapter III. Each specimen was placed in the TOPCON SM-510 scanning electron microscope specimen holder such that the specimen surface was at an angle of 70° relative to the incident electron beam. Five-hundred BKD patterns were

randomly captured from each specimen grip and, separately, from each gage section.

These were automatically indexed predominantly using the Hough transform incorporated in TSL's APR software. The indexed patterns were used to generate a set of three discrete pole figures for each region in order to preserve all the information obtained via BKD.

The discrete pole figures for the material with differing process histories but identical test temperatures are shown in Figure 4.1. The discrete figures obtained from the annealed grip sections, Figure 4.1 (a), (c), and (e), showed crystal normals that were substantially random. Rolling, as done in the processing here, is expected to produce a strong rolling texture and, normally, a recrystallized material will also exhibit a strong texture [Ref. 25]. When particles large enough to cause PSN are nucleation sites, however, the texture tends to become randomized as a result of local lattice rotations occurring around the particles during thermomechanical processing [Ref. 26]. The randomness of the discrete pole figures strongly suggests that recrystallization in this material originated by way of PSN. A slight preferred orientation is apparent upon close inspection of the {111} and {200} stereographic projections for the materials overaged at 400°C for either 50 or 100 hours. A low concentration of crystal normals is observed at the center of the {200} pole figures. These normals likely reflect a {001}<100> cube component in the recrystallized texture. The discrete figures from the grip section of the material overaged at 450°C for 100 hours revealed that for this overaging condition, the microtexture was more random.
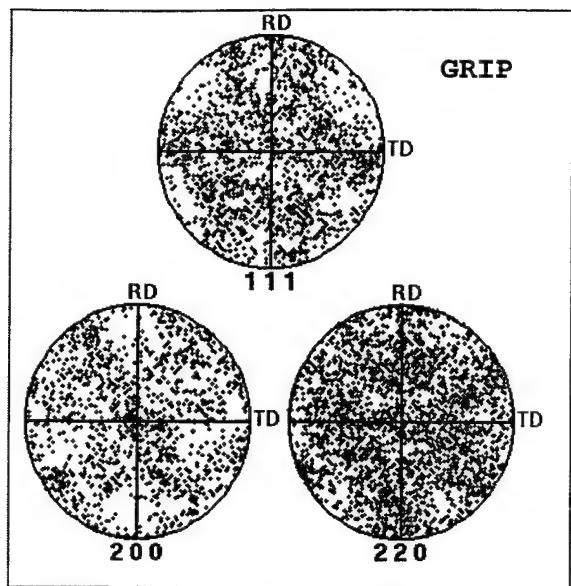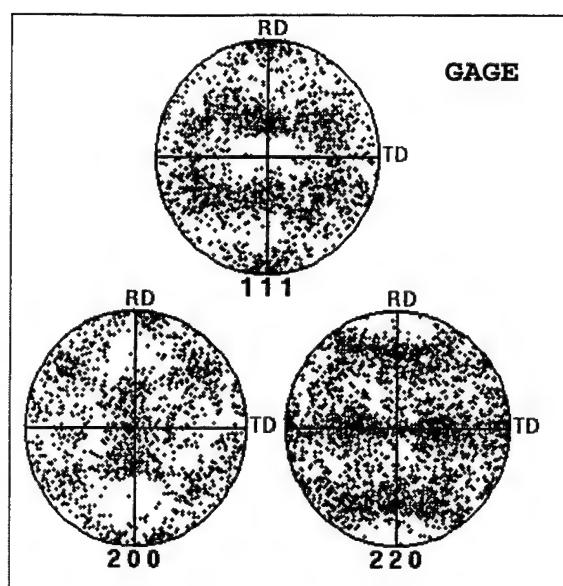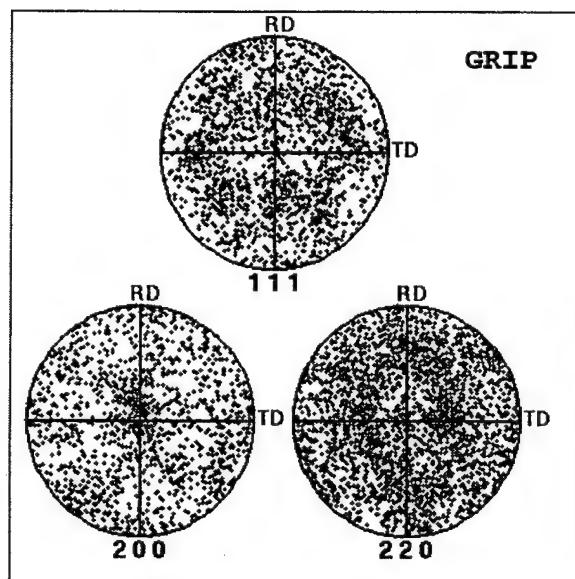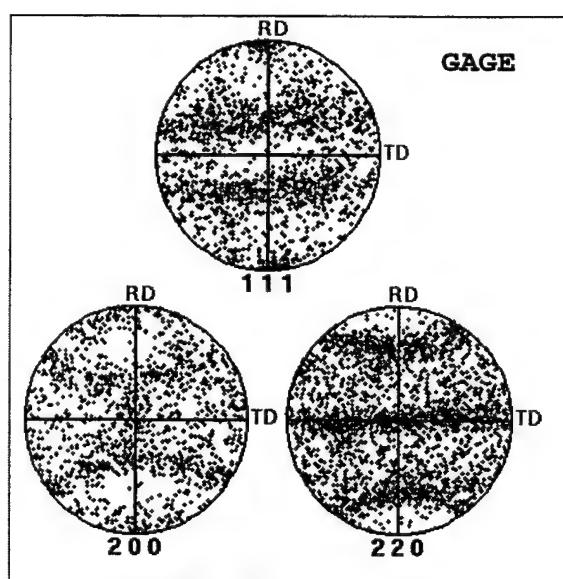
**Figure 4.1:** Discrete Pole Figures From Annealed Grip and Deformed Gage Sections for Material with Different Processing Histories. (a) and (b): Overaged at 400 Deg C for 50 Hours. (c) and (d): Overaged at 400 Deg C for 100 Hours. (e) and (f): Overaged at 450 Deg C for 100 Hours.
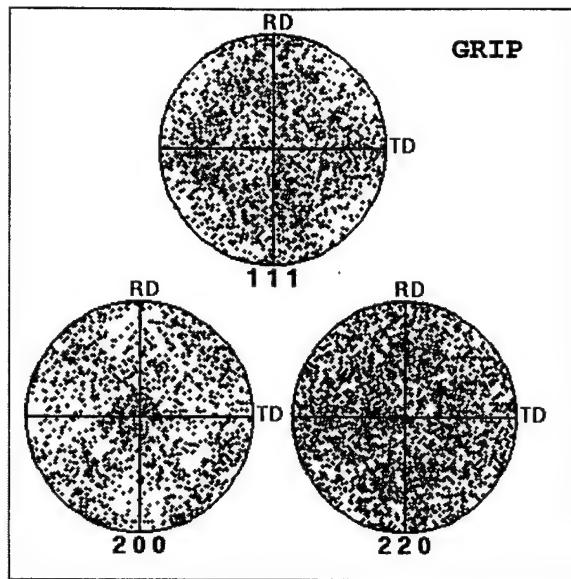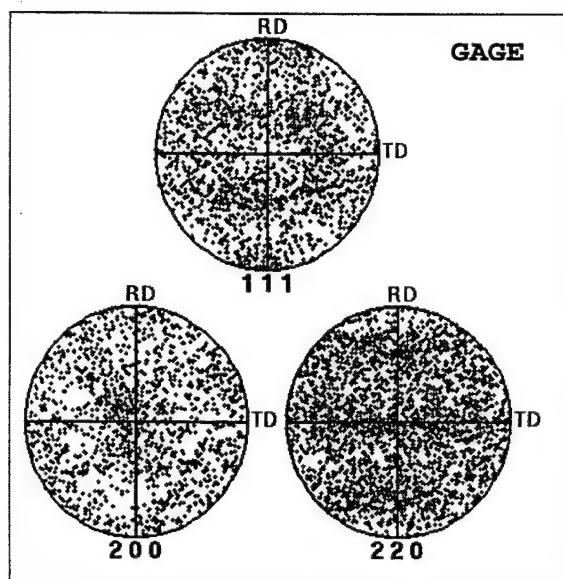
(e)   (f)

Figure 4.1 (Continued)

The discrete pole figures for the deformed gage sections in Figure 4.1 (b), (d), and

(f) were considerably different from those of the undeformed grip sections. For the two

materials overaged at 400°C prior to rolling, the discrete pole figures exhibit bands of

plotted normals that are consistent with <111> fiber textures. Such a <111> fiber texture

indicates multiple slip in the FCC structure of aluminum. Nevertheless, the ductility in

both cases was $\approx$ 188%, likely reflecting some contribution of grain boundary sliding in

the 21.0 μm grain size material. Upon overaging at 450°C for 100 hours, the deformation

occurred predominantly by grain boundary sliding instead of slip as reflected in a weaker

fiber texture. An increased contribution to the total strain by grain boundary sliding is

consistent with the finer 11.2 μm grain size attained in prior processing. However,

ductility increased only slightly to 196.4%; as noted by Peet [Ref. 20], cavitation also

became apparent. Suppression of this cavitation would likely lead to still larger

elongations.

2. Effect of Test Conditions

The effect of test conditions, including strain rate and temperature, on sample

elongation was examined for one specific thermomechanical process. The process of

interest was that which had produced the greatest ductility in the previous study: material

overaged at 450°C for 100 hours. Samples of the material, subjected to a strain rate of

10^{-4} sec^{-1} and test temperatures of 300, 400, and 450°C, were examined. As the test

temperature was increased, the material's ductility increased from about 140% to almost

300% (Figure 4.2). Table 4.1 also indicates that the true volume grain size decreased

when the test temperature increased from 300 to 400°C but increased again when the test
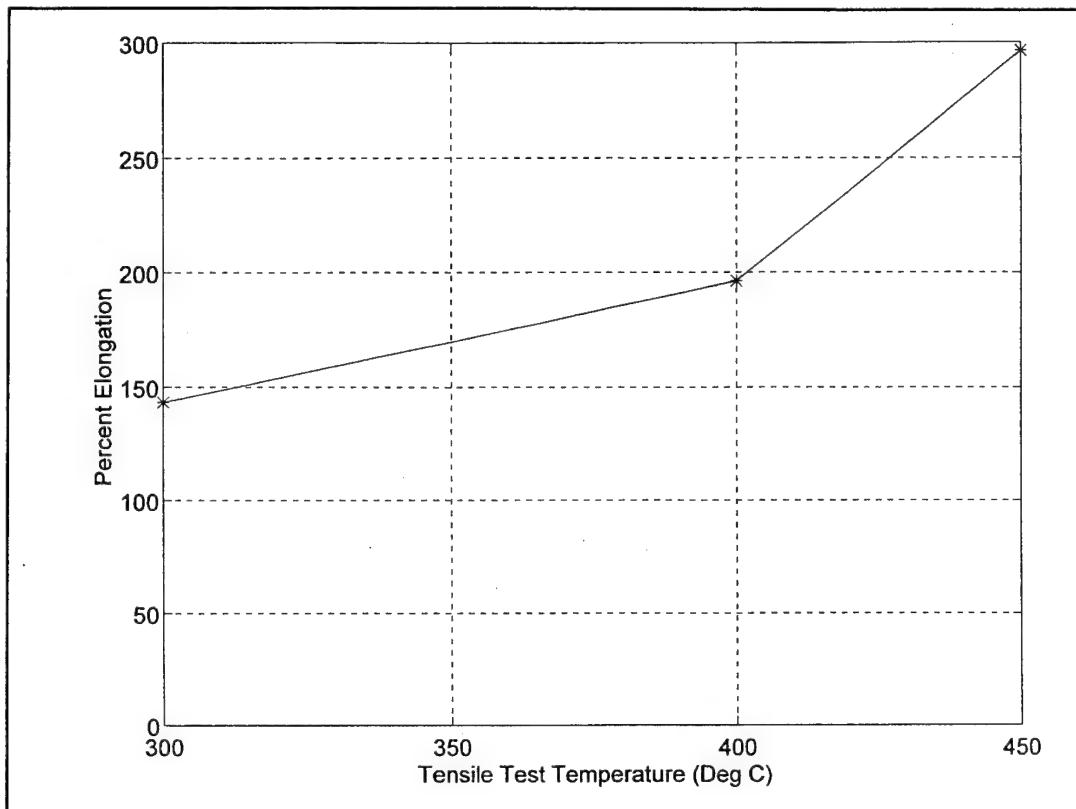
Figure 4.2: Ductility vs. Test Temperature

temperature was raised to 450°C. The increased grain size was likely a result of grain growth after recrystallization had been completed.

The discrete pole figures for the material with the same processing history but varying test conditions are compared in Figure 4.3. The plots for the material tested at 400°C is reproduced from Figure 4.1 to facilitate comparison.

The annealed grip section discrete pole figures in Figure 4.3 (a), (c), and (e) are very similar. Substantially random distributions of grain normals is evident in each of the discrete pole figures. Some evidence of the {001}<100> cube component in the {200} plot is seen for the material tested at 300°C. Even this component, however, essentially disappeared as the test temperature was increased to 400°C and above.
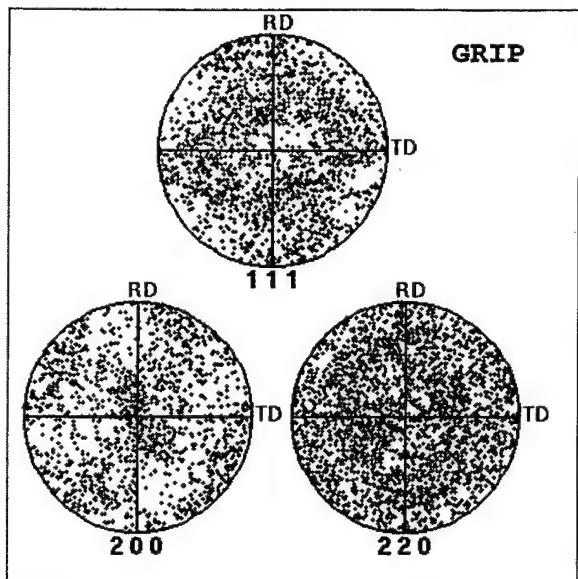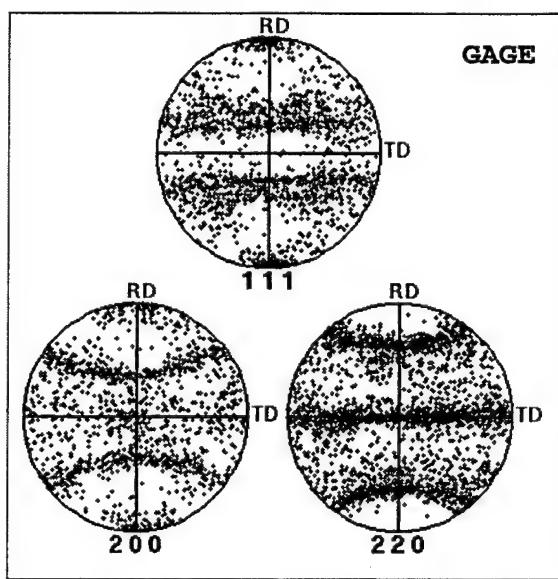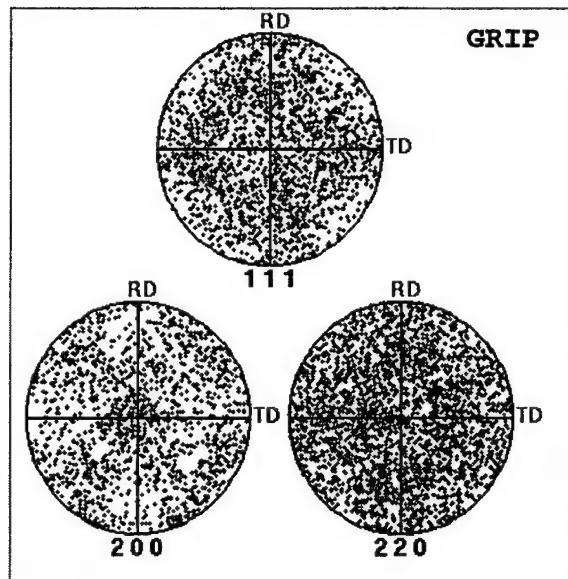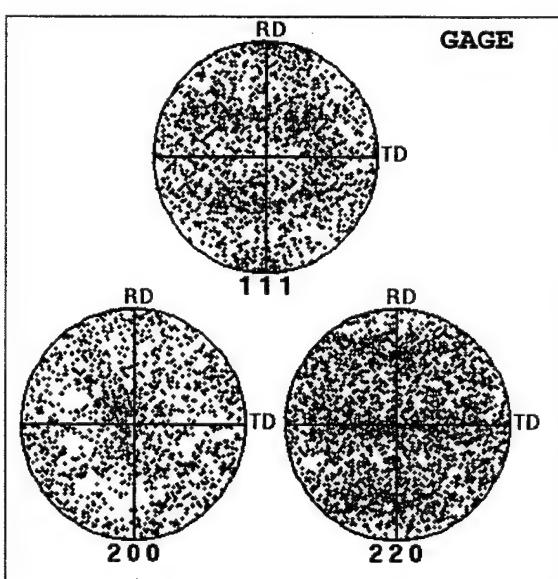
FIGURE 4.3: Discrete Pole Figures for Annealed Grip and Deformed Gage Sections for Material with the Same Processing History. Each Sample was Overaged at 450 Deg C for 100 Hours. (a) and (b): Tested at 300 Deg C. (c) and (d): Tested at 400 Deg C. (e) and (f): Tested at 450 Deg C.
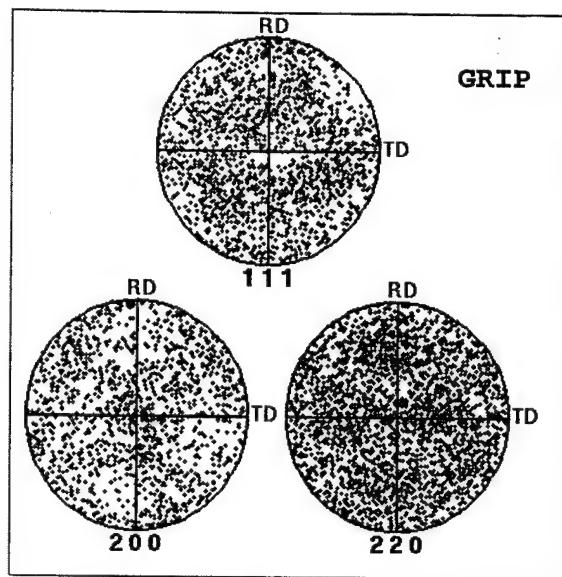
(e)
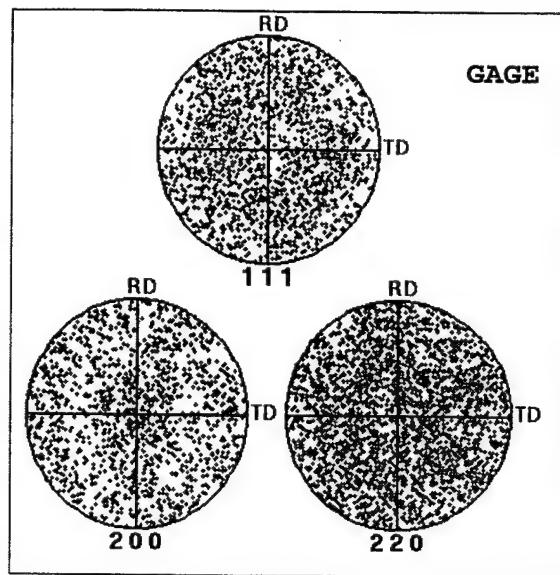
(f)

Figure 4.3 (Continued)

The discrete pole figures from the deformed gage section for the sample tensile tested at 300°C (Figure 4.3 (b)) exhibits a strong <111> fiber texture, indicating that deformation occurred via slip at this temperature. As the test temperature was increased to 400°C and then to 450°C , the fiber texture diminished and a random discrete plot was seen to develop (Figure 4.3 (d) and (f)) and ductility increased to 296.4% at the highest test temperature. The discrete pole figure for the most ductile material was essentially fully random with no discernible texture component in the deformed gage section.

3. Discussion

A partial phase diagram representing the Al end of the Al-Cu system is illustrated schematically in Figure 4.4. Tie lines are indicated for temperatures of 400 and 450°C; clearly, the equilibrium volume fraction of Θ is expected to decrease according to the lever rule as temperature increases from 400 to 450°C. Previous research by Peet [Ref. 20] indicated that, in general, the volume fraction of Θ, present in the form of overaged precipitate particles, decreased in Al 2519 as the overaging temperature increased. The quantitative results reported by Peet were consistently above theoretical values, apparently because the Θ phase stood in relief during electropolishing. Figure 4.5 represents schematically the expected effect of the overaging temperature and time on the size distribution of these Θ-phase particles. It is assumed that aging has lead to the equilibrium volume fraction for the temperature in question and that only precipitate coarsening is occurring. Superimposed as well is a value, $d_{p,crit}$, reflecting a critical size necessary for PSN of recrystallization.
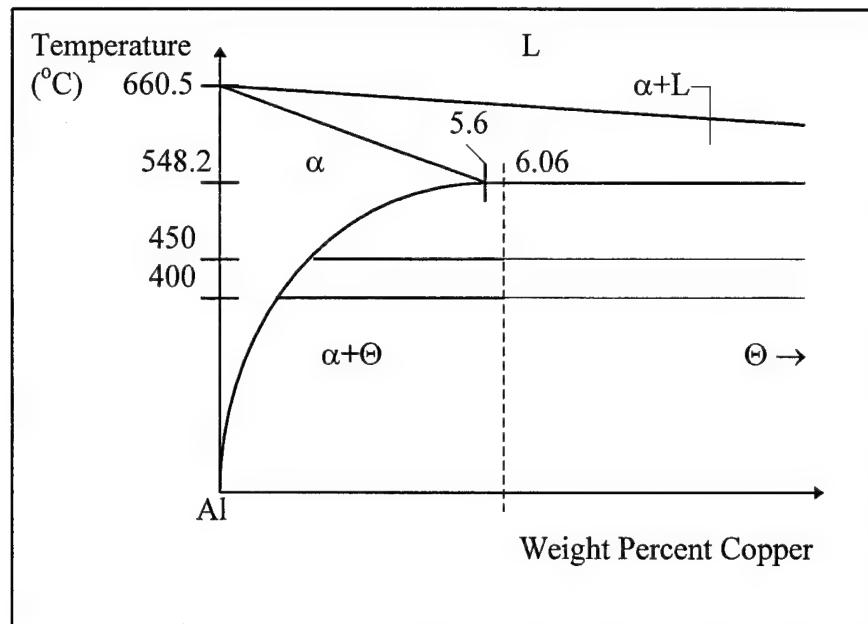
Figure 4.4: Section of Al-Cu Phase Diagram Showing Volume Fraction Decrease of
Θ-Phase for Increased Processing Temperature

It was hypothesized by Bohman [Ref. 17] that when the overaging time is
increased, the size distribution of precipitate particles shifts to a larger mean particle
diameter relative to $d_{p,crit}$. For the equilibrium volume fraction of Θ, the number of
particles exceeding $d_{p,crit}$ may increase in spite of the fact that the total number of
particles decreases. This would be beneficial in grain refinement because more
precipitate particles would be of a size above the critical diameter, thought to be 1-2μm
[Ref. 9], necessary for PSN. Thus, more grains would nucleate. The more numerous
grains would grow until impingement with neighboring grains, and this would result in a
finer grain size. Even though the volume fraction of the particles, determined by the
lever rule, decreased, the number of particles above a critical diameter, represented by the
area under the curve to the right of the critical particle size, would increase.
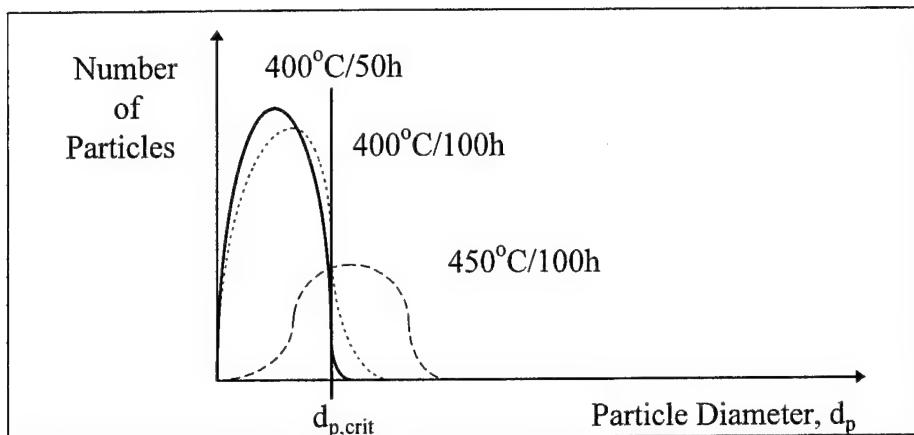
Figure 4.5: Precipitate Particle Size Distribution

Based on Figure 4.5, it is suggested that at an overaging temperature of 400°C, the volume fraction of Θ particles is relatively high, but the number of particles above the critical diameter is low. This leads to fewer precipitate particles being capable of nucleating grains, which resulted in a large grain size. As noted in this research, the material overaged at 400°C for 50 and 100 hours exhibited a grain size of 21.0 μm, the largest in the observed sample group. Increasing the overaging temperature to 450°C (for 100 hours), however, resulted in a final true volume grain size of 11.2 μm because an increased number of particles were activated to function as nucleation sites for recrystallization.

B. GRAIN REFINEMENT VIA INCREASED STRAIN

The second part of this research analyzed the role of total processing strain on grain refinement. The TMP that previously had resulted in the finest grain size was selected, but now the total processing strain was varied during the warm rolling phase of

the TMP. With the increased strain, more precipitate particles would be activated as nucleation sites for recrystallization according to the PSN model. Three new billets of Al 2519 were rolled in accordance with the rolling schedule in Table 3.2. One sample was rolled through the thirteenth pass, W13, while for another, processing was terminated after W15, and the third sample was rolled through W18. These three samples attained total processing strains of 1.4, 2.2, or 3.3, respectively. After processing, three samples from each processed material were sectioned and annealed at 400°C for either 0.5, 1.0, or 2.0 hours. Such recrystallization anneal times were selected to replicate the tensile test times that a specimen typically experienced when tested at strain rates of 10^{-2}, 10^{-3}, and 10^{-4} sec^{-1}, respectively. Each sample was then polished and observed with the SEM. Photomicrographs utilizing orientation contrast were taken to facilitate grain size analysis.

1. Microscopy

All photomicrographs are oriented with the rolling direction horizontal in the field of view. The SEM magnification was maintained at 1000X, the accelerating voltage was set at 5.0 kV (to enhance orientation contrast and minimize atomic number contrast with the Θ-phase particles), and the working distance was approximately 10 mm for all micrographs. In the micrographs, the aluminum grains were clearly visible and distinct at the low accelerating voltage. The Θ-phase particles stood out in the backscatter images because of their relatively high atomic number. A 20 μm bar is present on each photomicrograph to facilitate grain size measurements.

41

The material with a total processing strain of 1.4, subsequently annealed for 1.0 hour at 400°C, is shown in Figure 4.6. The true average grain size, D, was calculated to be 16.9 ± 1.7 μm with a 95% confidence level. Standard statistical methods were used to determine the mean and error values. Most grains were equiaxed, although some remained elongated in the rolling direction as a result of prior rolling. The precipitate particles were also elongated in the prior rolling direction.

Material with similar annealing conditions but a total processing strain of 2.2 is exhibited in Figure 4.7. The true average grain size, D, has decreased to 12.7 ± 1.0 μm (with a 95% confidence level) with this increased rolling strain. This was somewhat greater than the value reported by Peet [Ref. 20], 11.2 μm for nominally the same processing conditions. Although some of the grains appear elongated in the prior rolling direction, the majority of grains are equiaxed in shape. As a result of the increased strain, a larger number of precipitate particles were elliptical in shape with the major axis in the prior rolling direction.

A representative sample of the material with a total processing strain of 3.3 is shown in Figure 4.8. The true volume grain size was determined to be reduced to 9.2 ± 1.4 μm, with a 95% confidence level, which is substantially less than had been previously achieved with a total processing strain of 2.2. The aluminum matrix microstructure appeared very refined and equiaxed, but an increasing number of precipitate particles were deformed as a result of rolling.

2. Discussion

The computed true volume grain sizes for the material as a function of total processing strain and annealing time are listed in Table 4.2. The true volume grain size was not determined for all conditions, and these are designated by a "/" mark. The calculated true volume grain size data as a function of total processing strain and annealing time at 400°C is displayed in Figure 4.9.

Final Roll Pass #	Total Processing Strain	True Volume Grain Size (μm)		
		Anneal Time (hours) at 400°C		
		0.5	1.0	2.0
W13	1.4	/	16.9	/
W15	2.2	13.1	12.7	12.0
W18	3.3	10.8	9.2	10.3

Table 4.2: True Volume Grain Size as a Function of Total Processing Strain and Annealing Time at 400°C

Of primary interest is that the microstructure was refined as the total processing strain was increased for all annealing times. For the material with a total processing strain of 2.2, the true volume grain size decreased from an average of 13.1 μm after annealing for 0.5 hour to 12.0 μm after 2.0 hours. Although the computed grain size continuously decreased, the measurements fall within the 95% confidence interval for the material annealed for 1.0 hour, indicating the grain size to be statistically constant. Grain size reduction, however, could be accounted for by an increased number of grains nucleating as the annealing time increased.

All grain size measurements for the material with a 3.3 total processing strain were less than those with the 2.2 strain. Figure 4.9 shows that the true volume grain size
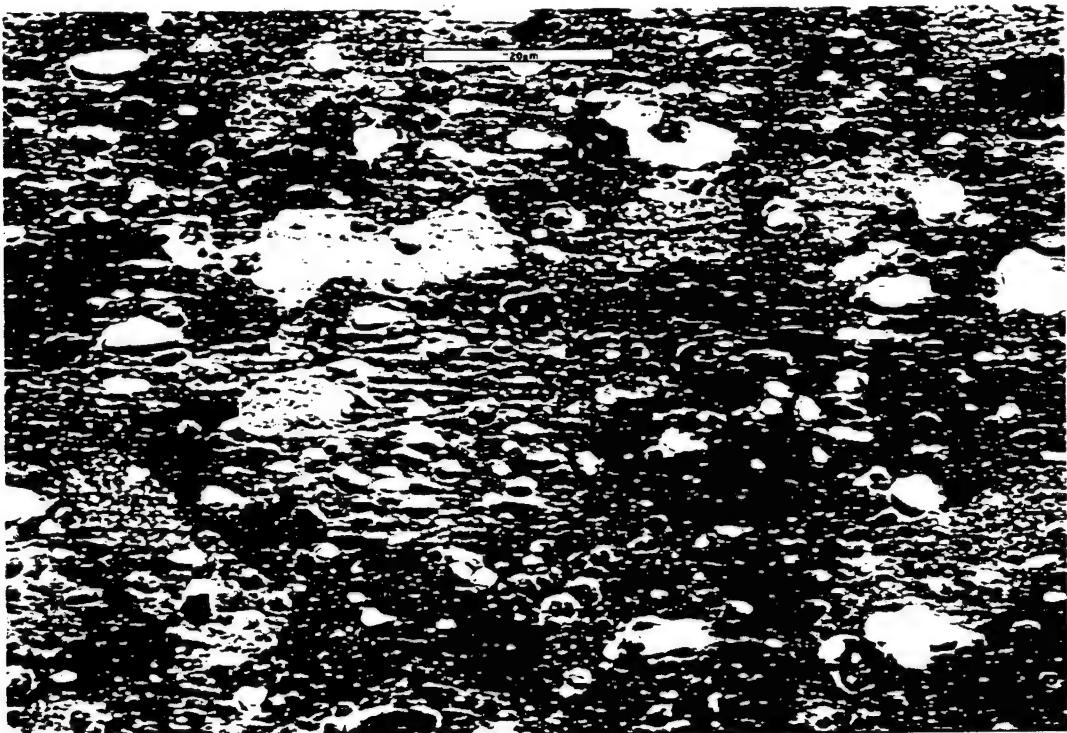
Figure 4.6: Microstructure for 1.4 Total Processing Strain
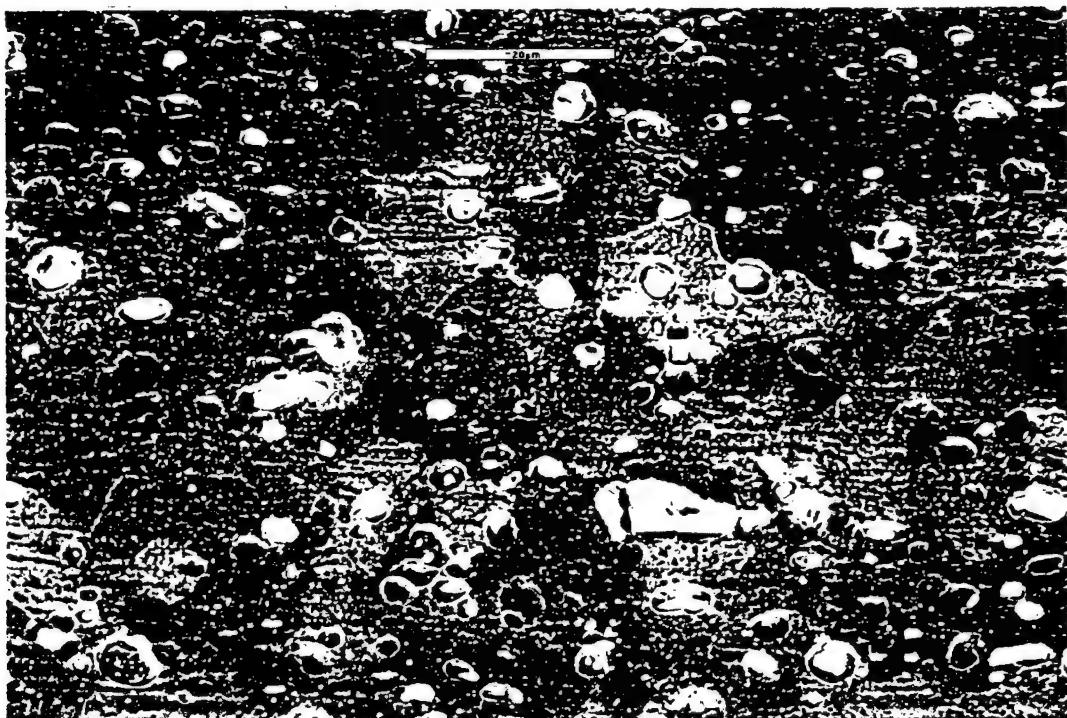
**Figure 4.7:** Microstructure for 2.2 Total Processing Strain
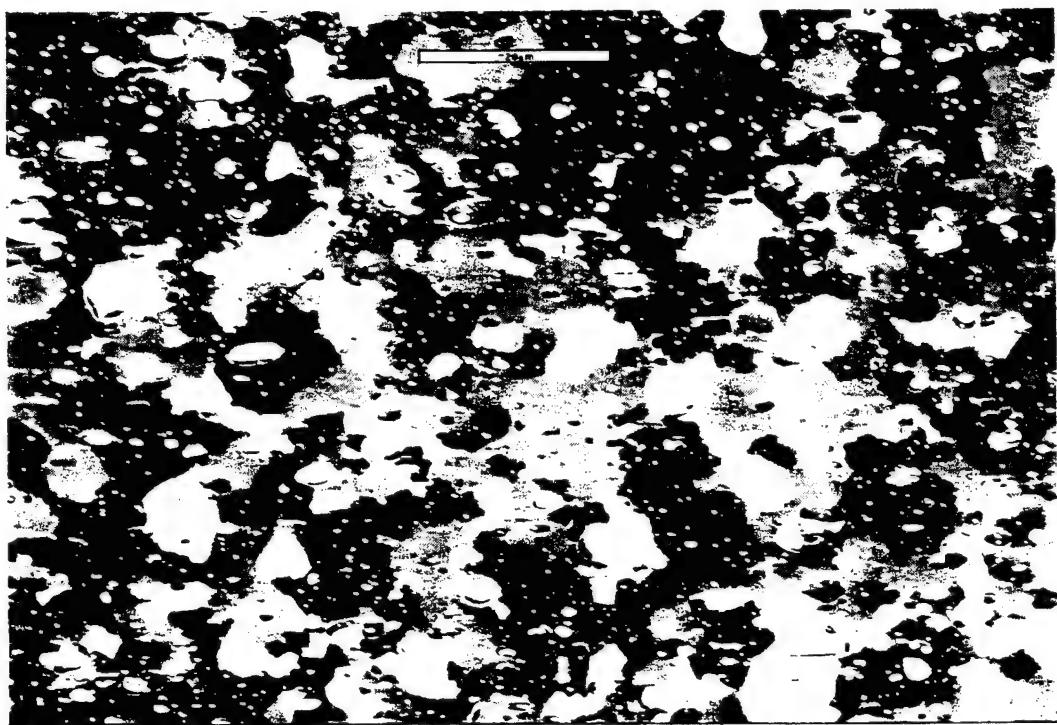
Figure 4.8: Microstructure for 3.3 Total Processing Strain
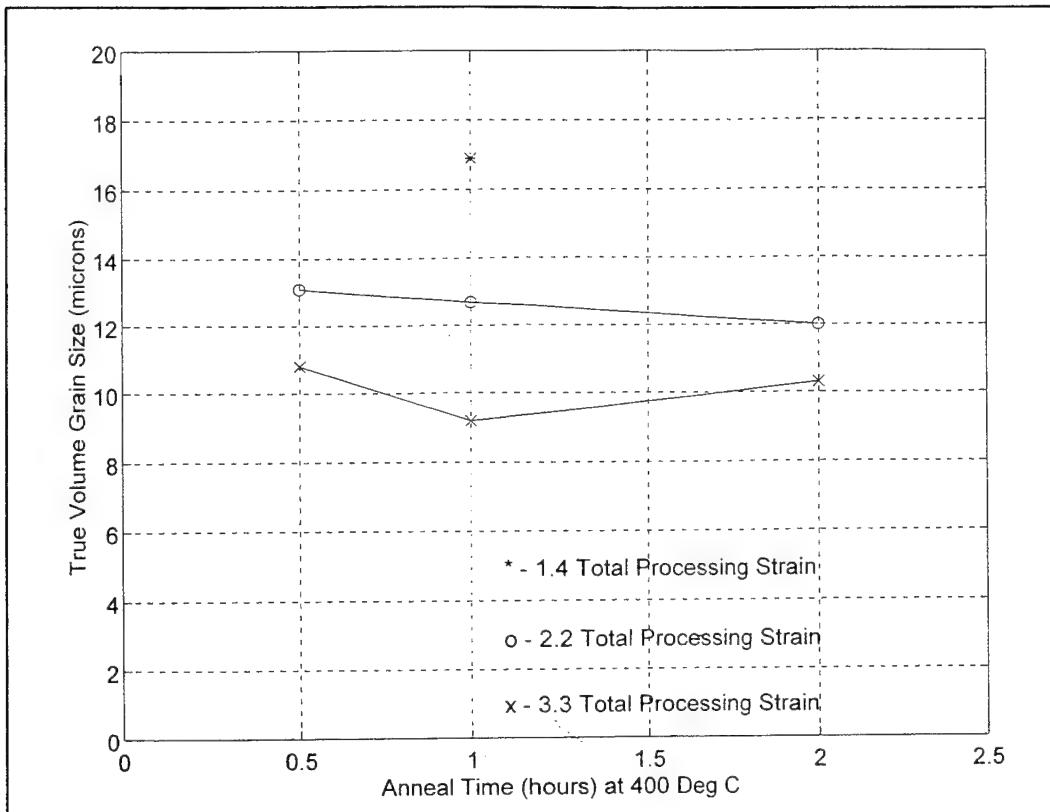
Figure 4.9: Graphical Representation of Table 4.2

initially decreased from 10.8 μm after a 0.5 hour anneal to 9.2 μm after 1.0 hour but then increased to 10.3 μm after 2.0 hours. Thus, the grain size is essentially constant within the accuracy of measurement although the material may have fully recrystallized after annealing for 1.0 hour at 400°C and grain growth had started. The material's recrystallization temperature, defined as the temperature when recrystallization is completed in 1.0 hour [Ref. 27], may be near 400°C.

The effect of increasing the total processing strain on the material annealed for 1.0 hour is shown in Figure 4.10. The true volume grain size continuously decreases from 16.9 to 9.2 μm as the processing strain was increased, and none of the 95% confidence

46
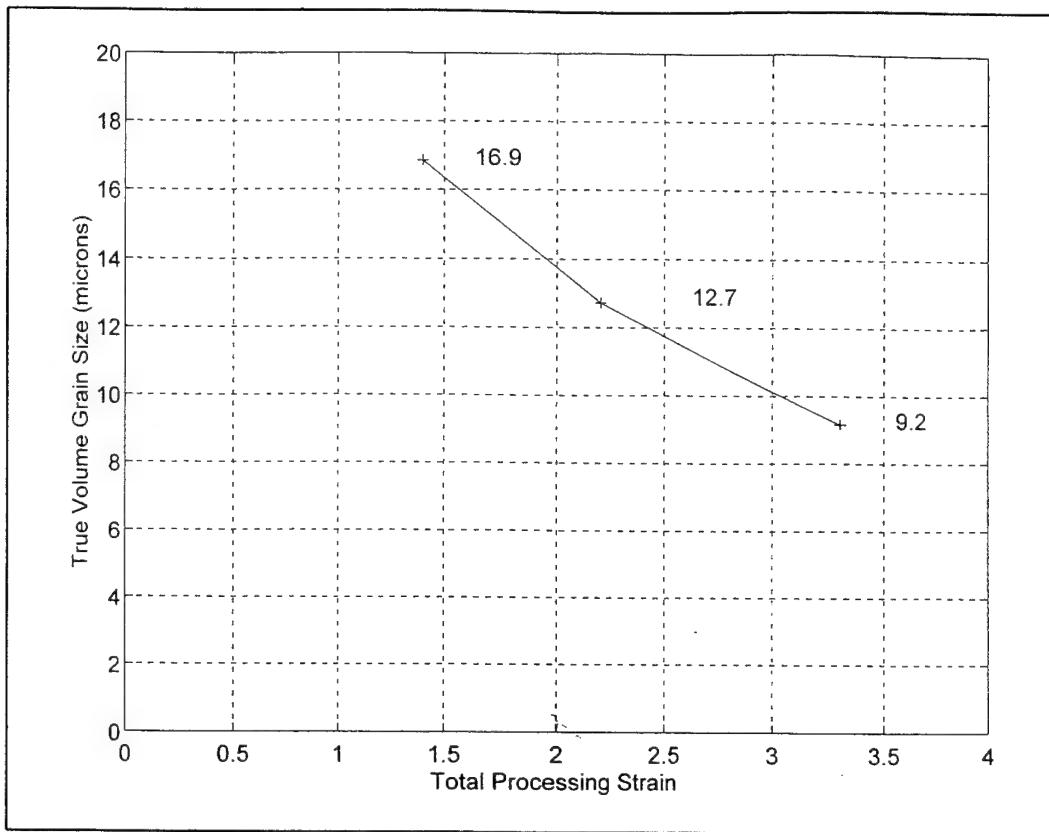
Figure 4.10: True Volume Grain Size vs. Total Processing Strain for Material Annealed for 1.0 Hour at 400°C

intervals overlap. These results are also in agreement with the PSN model shown in Figure 2.2 in which increased strain allows particles of a smaller size, $d_{p,crit}$, to function as sites for nucleation. This increases the number of particles available for PSN and ultimately leads to a finer grain size. The increased strain also produces more highly misoriented nuclei and increases the potential for growth. Together, these factors allow for finer particles to serve as nucleation sites as strain is increased, thereby decreasing the final grain size.

Volume fraction of Θ-phase was calculated for the material with the varying total processing strain. At approximately 20 volume percent, the results were higher than those obtained theoretically from the equilibrium phase diagram using the lever rule. The results, however, were consistent for each of the total processing strains and annealing conditions. It is believed that the precipitate particles stand in relief after electropolishing is performed on the material.

The material with the 3.3 total processing strain would be expected to provide the greatest superplastic response because of the more highly refined grain size, although cavitation may serve to limit ductility in these materials.

V. CONCLUSIONS AND RECOMMENDATIONS

A. CONCLUSIONS

The two major efforts of this thesis, discrete pole figure measurements and grain refinement through thermomechanical processing, have produced sufficient data to make the following conclusions:

1. The discrete pole figures of Peet's most superplastic material revealed a completely random grain orientation indicative of microstructure refinement by PSN of recrystallization. The random texture also indicated that the material deformed via grain boundary sliding, the mechanism characteristic of superplastic behavior. Cavitation around large precipitate particles and a larger than desired grain size were the limiting factors for this material's ductility.

2. When overaging time and temperature did not allow sufficient Θ-phase particles to grow to the requisite critical size, a coarser grain size was produced, and the discrete pole figures showed a fiber texture indicating that the primary mechanism of deformation was slip.

3. The PSN theory provides a basis for designing processes to achieve grain microstructure refinement. As the total processing strain was increased from 1.4 to 3.3, the true volume grain size decreased and attained a minimum of 9.2 μm for a post-processing anneal time of one hour at 400°C. Annealing for longer than one hour produced slightly larger grains as a possible consequence of grain growth. This refined microstructure can be expected to yield a superplastic response greater than previously obtained with Al 2519.

B. RECOMMENDATIONS

Follow on research in this area should concentrate on the following items:

1. Conduct mechanical testing on the material with a total processing strain of 2.2 and 3.3 at test temperatures of 400 and 450°C and strain rates 10^{-2}, 10^{-3}, and 10^{-4} sec^{-1}.

2. Develop sample preparation methods to allow the study of the size distribution of Θ-phase particles.

3. Vary overaging time material at 450°C as opposed to 400°C as well as total processing strain to determine the effect on grain size and subsequent superplastic ductility.

4. Consider the sequence of reductions during rolling to maximize the strain per pass in the final rolling passes. This will enhance the likelihood of PSN.

5. Seek optimized times and temperatures for overaging.

LIST OF REFERENCES

1. Edington, Jeff W., "Microstructural Aspects of Superplasticity," *Metallurgical Transactions*, Vol. 13A, pp. 703-715, 1982.

2. Hamilton, C. H., "NATO/AGARD Lecture Series on Superplasticity," *Superplastic Sheet Forming*, Washington State University, pp. 2.1-2.24, 1987.

3. McNelley, T. R., and Hales, S. J., "Superplastic Aluminum Alloys," *Naval Research Reviews*, Vol. 39.1, pp. 51-57, Office of Naval Research, 1987.

4. Product Information, Northrup Corporation, Hawthorne, CA, November 1983.

5. Baudelet, B., "Industrial Aspects of Superplasticity," *Material Science and Engineering*, A137, pp. 41-55, 1991.

6. "Binary Alloy Phase Diagrams," *American Society for Metals*, Vol. 1, Metals Park, Ohio, 1986.

7. Kou, S., Welding Metallurgy, John Wiley & Sons, New York, 1987.

8. *Metals Handbook*, 10th ed., Vol. 2, pp. 3-80, American Society for Metals, 1991.

9. Humphreys, F. J., "The Nucleation of Recrystallization at Second Phase Particles in Deformed Aluminum," *Acta Metallurgica*, Vol. 25, pp. 1323-1344, 1977.

10. Watts, B. M., Stowell, M. J., Baikie, B. L., and Owen, D. G. E., "Superplasticity in Al-Cu-Zr Alloys, Part II: Microstructural Study," *Metals Science Journal*, Vol. 10, No. 6, pp. 189-197, 1976.

11. Wert, J. A., "Grain Refinement and Grain Size Control," *Superplastic Aluminum Alloys*, edited by Paton, N. E., and Hamilton, C. H., pp. 69-83, Conference Proceedings, TMS-AIME, Warrendale, PA, 1982.

12. Pearce, R., "Superplasticity-an Overview," Cranfield Institute of Technology, Cranfield, 1986.

13. Ashby, M. F., *Philos Metall.*, 21 (1970) 399.

14. Argon, A. S., Im, J., and Safoglu, R., "Cavity Formation From Inclusions in Ductile Fracture," *Metallurgical Transactions*, Vol. 6A, p.82, 1975.

15. McNelley, T. R., Crooks, R., Kalu, P. N., Rogers, S. A., "Precipitation and Recrystallization During Processing of a Superplastic Al-10Mg-0.1Zr Alloy," *Material Science and Engineering*, A166, pp. 135-143, 1993.

16. Mathe, W., *Precipitate Coarsening During Overaging of 2519 Al-Cu Alloy: Application to Superplastic Response*, Master's Thesis, Naval Postgraduate School, Monterey, CA, March 1992.

17. Bohman, S., *Thermomechanical Processing of Aluminum Alloy for Grain Refinement and Superplasticity*, Master's Thesis, Naval Postgraduate School, Monterey, CA, June 1992.

18. Dunlap, J., *Study of Refinement in Al Alloy 2519 Using Backscatter Orientation - Contrast Made in the Scanning Electron Microscope*, Master's Thesis, Naval Postgraduate School, Monterey, CA, December 1992.

19. Zohorsky, P., *Study of Precipitation and Recrystallization of Al Alloy 2519 by Backscattered Electron Imaging Methods*, Master's Thesis, Naval Postgraduate School, Monterey, CA, September 1993.

20. Peet, B. *Thermomechanical Processing of an Al 2519 Alloy, and an Assessment of Its Superplastic* Response, Master's Thesis, Naval Postgraduate School, Monterey, CA, March 1995.

21. Culity, B. D., *Elements of X-Ray Diffraction*, Addison-Wiley, 1978.

22. Randle, V., Ralph, B., and Dingley, D., "The Relationship Between Microtexture and Grain Boundary Parameters," *Acta Metallurgica*, Vol. 36, pp. 267-273, 1988.

23. *ASM Handbook*, 10th ed., Vol. 4, pp. 823-880, American Society for Metals, 1991.

24. Humphreys, F. J., "Local Lattice Rotations at Second Phase Particles in Deformed Metals," *Acta Metallurgica*, Vol. 27, pp. 1801-1814, 1979.

25. Bricknell, R. H., and Edington, J. W., "Textures in a Superplastic AL-6Cu-0.3Zr Alloy," *Acta Metallurgica*, Vol. 27, pp. 1303-1311, 1979.

26. Hansen, N., and Jensen, J., "Deformation and Recrystallization Textures in Commercially Pure Aluminum," *Metallurgical Transactions*, Vol. 17A, pp. 253-259, 1986.

27. Callister, W. D., *Materials Science and Engineering: An Introduction*, 2nd Edition, John Wiley and Sons, Inc., New York, NY, 1984.

INITIAL DISTRIBUTION LIST

1.   Defense Technical Information Center 2
     8725 John J. Kingman Rd., STE 0944
     Ft. Belvoir, Virginia 22060-6218

2.   Library, Code 13 2
     Naval Postgraduate School
     Monterey, California 93943-5101

3.   Naval Engineering, Code 34 1
     Naval Postgraduate School
     Monterey, California 93943-5100

4.   Department Chairman, Code ME/Kk 1
     Department of Mechanical Engineering
     Naval Postgraduate School
     Monterey, California 93943-5000

5.   Professor T. R. McNelley, Code ME/Mc 4
     Department of Mechanical Engineering
     Naval Postgraduate School
     Monterey, California 93943-5000

6.   LT Steven L. Stancy, USN 1
     1208 W. Peterson Avenue
     Park Ridge, Illinois 60068